ATTITUDE STABILIZATION USING A ROTATING PLUG NOZZLE

by

John Emery Draim

MASSACHUSETTS INSTITUTE OF TECHNOLOGY
AEROPHYSICS LABORATORY

ATTITUDE STABILIZATION USING A ROTATING PLUG NOZZLE

[THESIS]

by

John E. Draim

Technical Report 158

Contract No. N00014-67-A-0204-0028
MIT DSR No. 71419

July 1969

Prepared for
Office of Naval Research
Dept. of the Navy
Washington, D.C.

ATTITUDE STABILIZATION USING A ROTATING PLUG NOZZLE

by

John Emery Draim
B.S., U.S. Naval Academy
(1949)

B.S. (Aero), U.S. Naval Postgraduate School
(1955)

S.M. (Aero), Massachusetts Institute of Technology
(1956)

SUBMITTED IN PARTIAL FULFILLMENT
OF THE REQUIREMENTS FOR THE DEGREE OF
ENGINEER OF AERONAUTICS AND ASTRONAUTICS

at the

MASSACHUSETTS INSTITUTE OF TECHNOLOGY
July 1969

ATTITUDE STABILIZATION USING A ROTATING PLUG NOZZLE

by

John E. Draim

Submitted to the Department of Aeronautics and Astronautics on July 11, 1969, in partial fulfillment of the requirements for the degree of Engineer of Aeronautics and Astronautics.

ABSTRACT

A modified plug nozzle in which the plug is spinning as a gyroscopic mass is investigated. It is postulated that exhaust gas flow is modulated between the plug and the rocket casing in such a manner as to provide a stabilizing moment around the rocket center of gravity, when the rocket longitudinal axis deviates from the plug-spin axis. Lagrange equations of motion are formulated for the dynamical system described by four generalized coordinates. These equations are mechanized in an analog computer to yield plots of rocket angular motions. Critical non-dimensional parameters for the system are identified and discussed. A small demonstrator model was designed, constructed and tested, first with a smooth conical plug, and then with a conical plug having indented turning slots in the area of the exhaust annulus. Tests conducted on the model demonstrated that sufficient gyroscopic rigidity can be generated to counter the unbalanced pressure field effects around the rotating plug. The fact that flow modulation does in fact generate a corrective moment around the rocket c.g. with angular deviation between the rocket and the plug-spin axes was also demonstrated. Model tests were conducted using compressed air up to 82 psia at the nozzle inlet. The

spherical pivot bearing is located away from the mainstream of exhaust gases; in this manner consideration was given to eventual problems associated with the effects of high temperature flow in an actual nozzle. It is concluded that within certain limits of the critical parameters, satisfactory attitude stabilization of a rocket vehicle can be realized using a rotating plug-type nozzle.

Thesis Supervisor: Eugene Covert
Title: Professor of Aeronautics and Astronautics

ACKNOWLEDGEMENTS

The author wishes to express his appreciation to his Thesis Supervisor, Professor Eugene E. Covert, for his guidance, helpful suggestions, and encouragement in all phases of a project which appeared highly speculative at the outset.

In addition, the author wishes to express his grateful appreciation to all members of the staff of the M.I.T. Aerophysics Laboratory for their assistance in carrying out experiments on the rotating plug nozzle. In particular, he would like to single out the following particular individuals who have rendered assistance in the areas indicated:

Dr. Michael Judd	Theoretical Analysis
Mr. Timothy Stephens	Instrumentation
Mr. Francis Harrow	Machining of Model
Mr. James Coffin	Test Setup and Test Operations
Mr. Charles Hawks	Test Rig Construction and Test Operations
Mr. Salvatore Albano	Test Rig Construction and Test Operations
Mr. John Goss	Materiel Procurement
Mr. William Byrne	Administrative and Contracts Assistance
Mrs. Catherine Callahan	Drafting Assistance
Miss Patricia O'Connor	Typing
Miss Helen Putnam	Typing
Mr. John Barley*	Analog Computer Runs
Mr. Kenneth Draim@	Data Reduction (Counting taped rpm pulses)

@Center Elementary School, Bedford, Mass.

*Technical Instructor, Dept of Aero and Astro, M.I.T.

The opportunity of conducting full-time graduate study at M.I.T. was made possible by the Bureau of Naval Personnel, Navy Department, Washington, D.C. The author feels a profound debt of gratitude for this opportunity to broaden his technical education, at an advanced stage in his career.

This research was sponsored by the Office of Naval Research under Contract No. N00014-67-A-0204-0028; Project No. NR 094-362/10-9-68 (473). Reproduction in whole or in part is permitted for any purpose of the United States Government.

TABLE OF CONTENTS

Chapter		Page
1.	INTRODUCTION.	1
	1.1 Situations Requiring Rocket Vehicle Attitude Stabilization	1
	1.2 Principle of the Rotating Plug Type Nozzle	2
	1.3 Anticipated Problem Areas.	4
	1.4 Method of Researching Rotating Plug Nozzle Feasibility	4
2.	THEORY OF THE ROTATING PLUG NOZZLE.	5
	2.1 Similarity of the Rotating Plug Nozzle to the Gyroscope and Top.	5
	2.2 Formulation of Lagrange Equations of Motion.	5
	2.3 Simplified Form of Lagrange Equations.	10
3.	ANALOG COMPUTER SIMULATION.	11
	3.1 Method of Simulation	11
	3.2 Discussion of System Dynamics.	12
	3.3 Discussion of Critical Parameters. . . .	13
4.	AERODYNAMIC PRESSURE FIELD AROUND THE ROTATING PLUG	17
	4.1 Plug Nozzle Flow	17
	4.2 Upsetting Moment Due to Plug-Rocket Angular Offset	18
5.	MODEL DESIGN AND CONSTRUCTION	20
	5.1 Design Philosophy.	20
	5.2 Design of Rotating Plugs	21
	5.3 Design of Ducting.	22
	5.4 Design of the Test Rig	22

TABLE OF CONTENTS (Continued)

Chapter		Page
6.	INSTRUMENTATION	24
	6.1 Measured Parameters	24
	6.2 Measurement Circuitry	24
	6.3 Calibration of Instrumentation	25
7.	TEST RESULTS	27
	7.1 General Outline of Tests	27
	7.2 Spin-Down Tests	27
	7.3 Side Force Measurements	28
	7.4 Preliminary Free-Spin Tests, Plug #1	28
	7.5 Final Series Free-Spin Tests	30
	7.6 Determination of K_p from Experimental Results	34
	7.7 Critical Frequencies of Spinning Tops and Spinning Plugs	35
	7.8 Estimation of Model Plug Equilibrium RPM	37
8.	CONCLUSIONS AND RECOMMENDATIONS	39
	8.1 Conclusions	39
	8.2 Recommendations	40
APPENDIX A		42
BIBLIOGRAPHY		71

LIST OF SYMBOLS

ϕ	angle between rocket longitudinal and xz-inertial plane, measured around z-axis
θ	angle between rocket longitudinal and z-inertial axis
ψ	angle of rotation around rocket, or plug, axis of symmetry
ζ	rocket damping ratio (non-dim.)(eq 3.10)
I_1, I_2	transverse moment of inertia (slug-ft^2)
I_3	spin moment of inertia (slug-ft^2)
K_p	plug constant, moment on plug per radian angular deviation from rocket axis (ft-lb/rad)
K_R	rocket constant, combined moment on rocket from aerodynamic fin and rocket nozzle side forces, around rocket c.g. (ft-lb/rad)
K_D	rocket damping factor (ft-lb-sec/rad)
H	plug angular momentum (ft-lb-sec)
M_ϕ, M_θ	external disturbing moments applied to rocket body (ft-lb)
T_p	plug time constant (sec)(eq 3.6)
T_R	rocket time constant (sec) (eq 3.5)
T_M	moment time constant (sec) (eq 3.7)
γ	non-dimensional parameter = T_R/T_p (eq 3.8)
μ	non-dimensional parameter = T_R/T_M (eq 3.9)
M_u	upsetting moment (ft-lb) (Fig 6)
M_T	trimming moment (ft-lb) (Fig 6)
M_S	spinning moment (ft-lb) (Fig 6)
M_C	centering moment (ft-lb) (Fig 6)

Subscripts

1	refers to rocket
2	refers to plug

LIST OF ILLUSTRATIONS

Figure		Page
1.	Rotating plug nozzle - schematic	43
2.	Rocket-plug coordinate system.	44
3.	M_R and M_P vector moment representation	44
4.	Analog computer set-up: rotating plug nozzle	45
5.	Rocket angle plots, $\phi_1(0) = 0.025$ rad, $\theta_1(0) = 0.025$ rad/sec.	46
6.	Rocket rotated around x-axis, showing various moments, M_V = upsetting moment, M_T = trimming moment, M_S = spinning moment, M_C = centering moment	50
7.	Plug nozzle, assembled	51
8.	Plug nozzle, disassembled.	52
9.	Plug #1 and Plug #2.	53
10.	Plug #1, design details.	54
11.	Plug #2, design details.	55
12.	Cage, design details	56
13.	Casing, design details	57
14.	Orifice plate, design details.	58
15.	Plug nozzle test rig	59
16.	Photocell instrumentation package, disassembled	60
17.	Photocell instrumentation package, assembled.	61
18.	RPM circuit diagram.	62

LIST OF ILLUSTRATIONS (Continued)

Figure		Page
19.	Plug angle circuit diagram	62
20.	Instrumentation assembled, on casing	63
21.	Pressure transducer power supply and angle/ RPM circuits	64
22.	Plug #1 spin-down test (bearing unloaded), (light spindle oil)	65
23.	Corrective side force vs. plug angular offset (Plug #1)	65
24.	Run no. 4, measured data	66
25.	Run no. 5, measured data	67
26.	Run no. 12, measured data	68
27.	Run no. 14, measured data	69
28.	Plug #2 equilibrium RPM (using Mangelsdorf method)	70

CHAPTER 1

INTRODUCTION

1.1 Situations Requiring Rocket Vehicle Attitude Stabilization

There are numerous requirements in rocketry for maintaining a rocket along a fixed axis during thrusting. Several examples are:

(a) Military rockets

(b) Upper stages of orbital boosters

(c) Scientific probe type rockets

In the first and second examples given above, it is not uncommon to find that the entire rocket is spun around its longitudinal axis by auxiliary means before main ignition occurs. In the third example, a very high launch tower is often used to guide the rocket during the first few seconds of acceleration. Subsequently, aerodynamically induced spin is commonly used. This approach is often used to overcome the large "tip-off" angles resulting from wind shears. In some cases, this spinning of the entire rocket may lead to additional problems, such as pitch-roll "lock-in", undesirable Magnus forces, structural problems, etc. All of these various approaches are used to control the trajectory, and hold down impact dispersion patterns.

For probe rockets having moderately high performance, the use of gyro platforms and servo driven attitude control systems is becoming more common[1]. Unfortunately, this approach results in a much more complicated and expensive vehicle. The system proposed in this study is aimed

at providing a simple, mechanical, attitude control device operable during rocket thrusting.

1.2 Principle of the Rotating Plug Type Nozzle (Patent Applied For)

Plug nozzles of the non-rotating type are basically similar to conventional convergent-divergent nozzles, in the principle of thrust generation. The significant difference is that the supersonic expansion in a plug nozzle is not confined within solid walls. Rather, gas flow is continuously redirected by the ambient pressure to produce an essentially axial velocity vector. The theory of plug nozzles has been fairly well developed, and they have been found to have an almost identical efficiency as conventional nozzles at the design pressure ratio[2]. In addition, they have been found to maintain a high efficiency over a much wider range of off-design pressure ratios than conventional nozzles. To date, however, plug nozzles have not been widely used. The main reason for this is the problem of erosion of the annular throat area by rocket gases and solid combustion products at high temperatures. This problem is more severe in a plug nozzle than in a conventional nozzle, but hopefully will be resolved by new materials and techniques. It is of interest to note that solid-propellant plug nozzles have been successfully test fired for short periods of time. (These nozzles had fixed, non-spinning plugs, of course)[3]. Even less well-developed than plug nozzle technology are control devices suitable for use on plug nozzles.

The rotating-plug nozzle is an application of basic mechanical gyro theory to the geometry of the plug nozzle. A plug spinning rapidly around its axis of symmetry would assume the characteristics of a gyro. By utilizing the

gyroscopic rigidity of the spinning plug and the favorable geometry of the system, gas flow can be modulated between the rocket casing and the rotating plug (see Fig. 1). The plug is supported centrally so as to permit rotation about two orthogonal axes perpendicular to the rocket longitudinal axis, as well as the rapid spin about the plug axis of symmetry. The means of support could thus be a single, spherical bearing, centrally located within the plug. Or, alternatively, the plug might be mounted using a universal joint; a conventional ball bearing would surround this universal joint to permit the high rotational speeds.

Plug spin-up could be accomplished by several means. Perhaps the simplest method would be to use the rocket exhaust itself, and spin the plug using vanes or slots exposed to the exhaust stream. A variation of this method would be to machine nozzles within the plug itself, with the necessary angular offsets and exhaust ports located downstream of the annulus in a low-pressure area. Still another method would be to use an external power source to spin up the plug, prior to establishing the main thrusting flow through the annulus. For example, an electric induction motor might be used , with the plug acting as the rotor. In all of the above cases, the plug could be retained on an alignment shaft during spin-up so as to maintain the desired spin axis.

As the rocket casing deviates from the desired (plug-spin) axis, a modulation of the exhaust annulus occurs. Because of the geometry of the plug and its centrally located point of support, a higher rate of gas flow occurs on one side of the annulus than on the other. This gives rise to a side force, hence a corrective moment on the rocket about its center of gravity. In essence, the effective thrust vector is offset so as to correct the system deviation.

A good analogy to the operation of the system would be a man balancing a long pole in his outstretched hand. As the pole deviates from the desired vertical attitude, the man supplies a side force and moment around the pole c.g. which tends to return the pole to the vertical.

1.3 Anticipated Problem Areas

A basic question which must be resolved is the overall effect of the pressure field and surface shears resulting from gas flow past the rotating plug. Any net moments which are generated by these forces will tend to alter the spin axis of the gyroscopic mass (rotating plug). The gyroscopic mass is intended to be a stabilizer for the system; it should act as a filter which reacts slowly to disturbances or rocket motions so that overall system dynamics remain within acceptable limits.

A second problem area, not considered in detail in this study, involves the adverse effects of the hot rocket exhaust gases. It is probable that this problem could be attacked using a variety of techniques used at present in the design and manufacture of turbojet aircraft engines. The most obvious design solution consists of isolating the plug bearing from the mainstream of exhaust gases. This has been accomplished in the design of the demonstrator model. Means of heat dissipation employing conduction or convection could also be employed.

1.4 Method of Researching Rotating Plug Nozzle Feasibility

The complexity of the pressure field effects on the rotating plug became apparent at the outset of this study. For this reason, it was considered desirable to perform both theoretical studies and experimental runs on a small demonstrator nozzle concurrently.

CHAPTER 2

THEORY OF THE ROTATING PLUG NOZZLE

2.1 Similarity of the Rotating Plug Nozzle to the Gyroscope and Top

The similarity of the rotating plug nozzle to the top is quite striking. In fact, it was this similarity in shape which led directly to the concept. It was hoped that the favorable geometric layout, coupled with a high degree of gyroscopic rigidity (high angular momentum) could lead to a workable system. References on the theory of the top proved to be helpful in setting up the dynamics problem on the analog computer and in interpreting the observed results[4,5].

2.2 Formulation of Lagrange Equations of Motion

Consider the spherical coordinate system of Fig. 2, with both the rocket and plug axes lying approximately in the horizontal plane. Hamilton's Principle and the Lagrange Equations are used to formulate the equations of motion of the system.

The following assumptions are made, in order to keep the mathematics manageable yet still adequately describe the overall system:

a. The rotating plug is suspended on a spherical bearing at the plug c.g. and has three degrees of rotational freedom.

b. Principle moments of inertia through the plug

c.g. are approximately equal; i.e.,

$$I_{P_1} = I_{P_2} \cong I_{P_3} = I_P$$

c. The plug is spinning rapidly about its axis of symmetry, with a constant spin rate; i.e.,

$$\dot{\psi}_2 = CONST$$

d. The rocket c.g. is located at the origin of the coordinate system and the rocket is free to rotate around two axes perpendicular to the rocket longitudinal axis, giving rise to angles ϕ_1 and θ_1.

e. The rocket is not spinning; i.e.,

$$\dot{\psi}_1 = 0$$

f. The transverse rocket moment of inertia is designated I_R, and includes the mass of the plug considered concentrated at the pivot point: the rocket moment of inertia about its longitudinal axis is very small compared with the transverse moment of inertia; i.e.,

$$I_{R_3} \ll I_R$$

Using the subscript '1' to denote the rocket and the subscript '2' to denote the plug, the total kinetic energy of the system is written:

$$T = \tfrac{1}{2} I_R (\dot{\theta}_1^2 + \dot{\phi}_1^2 \sin^2\theta_1) + \tfrac{1}{2} I_P (\dot{\theta}_2^2 + \dot{\phi}_2^2 \sin^2\theta_2) + \tfrac{1}{2} I_{R_3} (\dot{\psi}_1 + \dot{\phi}_1 \cos\theta_1)^2 + \tfrac{1}{2} I_P (\dot{\psi}_2 + \dot{\phi}_2 \cos\theta_2)^2 \qquad (2.1)$$

The third term above becomes vanishingly small because of assumption 2.2f, and (since ψ_2 is constant) the resulting

equation expresses the total system kinetic energy in terms of the four generalized coordinates, $q_i = \phi_1, \theta_1, \phi_2, \theta_2$.

Next, it is necessary to determine the generalized forces, Q_i. Since a non-conservative force field exists, we must use Hamilton's Principle in its most general form in writing the Lagrange Equations[6].

$$\int_{t_1}^{t_2} \left(\delta T + \vec{Q}_{i_{N.C.}} \cdot \vec{\delta q_i} \right) dt = 0 \tag{2.2}$$

It is possible to express the work done by the force system in the small displacements, $\delta\theta_1, \delta\theta_2, \delta\phi_1, \delta\phi_2$. Here, we assume that the moment on either the plug or the rocket is approximately a linear function of the angle between the plug and the rocket. An additional dissipative, or damping, moment, is exerted on the rocket due to aerodynamic and/or "jet-damping"[7] terms. These terms are assumed to be proportional to the first power of rocket angular velocity. In addition, for generality, external steady-state moments M_{ϕ_1} and M_{θ_1} are applied to the rocket. Denoting the thrust vector moment applied to the rocket by the action of the plug as $\vec{M}_R$, the aerodynamic vector moment applied to the plug by the pressure flow field as $\vec{M}_P$, and referring to Fig. 3, we may write:

$$\vec{M}_R = K_R \left(\vec{I}_R \times \vec{I}_P \right) \tag{2.3}$$

$$\vec{M}_P = K_P \left(\vec{I}_R \times \vec{I}_P \right) \tag{2.4}$$

Taking the ϕ and θ components separately the expressions for the generalized forces, Q_i, become:

$$M_{R_{\phi_1}} \delta\phi_1 = \{ K_R(\phi_2 - \phi_1) - K_D \dot{\phi}_1 + M_{\phi_1} \} \sin\theta_1 \delta\phi_1 = Q_1 \delta\phi_1 \tag{2.5}$$

$$M_{R_{\theta_1}} \delta\theta_1 = \{ K_R(\theta_2 - \theta_1) - K_D \dot{\theta}_1 + M_{\theta_1} \} \delta\theta_1 = Q_2 \delta\theta_1 \tag{2.6}$$

$$M_{R_{\phi_2}} = 0 \tag{2.7}$$

$$M_{R_{\theta_2}} = 0 \tag{2.8}$$

Similarly,

$$M_{P_{\phi_2}} \delta\phi_2 = K_P(\phi_2 - \phi_1) \sin\theta_2 \delta\phi_2 = Q_3 \delta\phi_2 \tag{2.9}$$

$$M_{P_{\theta_2}} \delta\theta_2 = K_P(\theta_2 - \theta_1) \delta\theta_2 = Q_4 \delta\theta_2 \tag{2.10}$$

$$M_{P_{\phi_1}} = 0 \tag{2.11}$$

$$M_{P_{\theta_1}} = 0 \tag{2.12}$$

Now, since the variations of the 4 q's (generalized coordinates) are independent, the generalized Lagrange equations are valid even though the system is non-conservative, i.e.;

$$\frac{d}{dt}\left(\frac{\partial T}{\partial \dot{q}_i}\right) - \frac{\partial T}{\partial q_i} = Q_i \tag{2.13}$$

From Eqs. (1) and (13) we may write:

$$\frac{d}{dt}\left(I_R \dot{\phi}_1 \sin^2\theta_1\right) - 0 = K_R(\phi_2 - \phi_1)\sin\theta_1 - K_D\dot{\phi}_1 \sin\theta_1 + M_{\phi_1}\sin\theta_1$$

$$I_R\left\{\ddot{\phi}_1 \sin\theta_1 + 2\cos\theta_1(\dot{\theta}_1)(\dot{\phi}_1)\right\} = K_R(\phi_2 - \phi_1) - K_D\dot{\phi}_1 + M_{\phi_1} \tag{2.14}$$

$$\frac{d}{dt}(I_R\dot{\theta}_1) - I_R \sin\theta_1\cos\theta_1(\dot{\phi}_1)^2 = K_R(\theta_2 - \theta_1) - K_D\dot{\theta}_1 + M_{\theta_1}$$

$$I_R\ddot{\theta}_1 - I_R\sin\theta_1\cos\theta_1(\dot{\phi}_1)^2 = K_R(\theta_2 - \theta_1) - K_D\dot{\theta}_1 + M_{\theta_1} \tag{2.15}$$

$$\frac{d}{dt}\left\{I_P\dot{\phi}_2\sin^2\theta_2\right\} + I_P\left\{(\dot{\psi}_2 + \dot{\phi}_2\cos\theta_2)\cos\theta_2\right\} = K_P(\phi_2 - \phi_1)\sin\theta_2$$

which reduces to:

$$I_P\ddot{\phi}_2 - I_P\sin\theta_2(\dot{\psi}_2)(\dot{\theta}_2) = K_P(\phi_2 - \phi_1)\sin\theta_2$$

also, since the rocket is oriented horizontally, $\sin\theta_2 \cong 1$. Substituting $I_P\dot{\psi}_2 = H$ = (angular momentum of plug, assumed constant).

$$I_P\ddot{\phi}_2 - H\dot{\theta}_2 = K_P(\phi_2 - \phi_1) \tag{2.16}$$

In a similar manner, we obtain:

$$I_P\ddot{\theta}_2 + H\dot{\phi}_2 = K_P(\theta_2 - \theta_1) \tag{2.17}$$

The above development yields a system of coupled ordinary linear differential equations. The characteristic equation of the system is of positive semi-definite form, so system stability is not automatically ensured.

2.3 Simplified Form of Lagrange Equations

In Eqs. (2.14) through (2.17) we make the further assumption that the cos $\theta_1(\dot{\phi}_1)^2$ and cos $\theta_1(\dot{\phi}_1)(\dot{\theta}_1)$ terms are negligibly small, and arrive at a simplified form of the Lagrange Equations:

$$I_R \ddot{\phi}_1 = K_R(\phi_2 - \phi_1) - K_D \dot{\phi}_1 + M_{\phi_1} \tag{2.18}$$

$$I_R \ddot{\theta}_1 = K_R(\theta_2 - \theta_1) - K_D \dot{\theta}_1 + M_{\theta_1} \tag{2.19}$$

$$I_P \ddot{\phi}_2 = H\dot{\theta}_2 + K_P(\phi_2 - \phi_1) \tag{2.20}$$

$$I_P \ddot{\theta}_2 = -H\dot{\phi}_2 + K_P(\theta_2 - \theta_1) \tag{2.21}$$

CHAPTER 3

ANALOG COMPUTER SIMULATION

3.1 Method of Simulation

The Lagrange equations of motion (2.18),(2.19),(2.20) and (2.21) were mechanized in a Pace Associates Inc., TR-48 analog computer. Various parameters such as K_P,K_R, H, etc., were selected to approximate ranges of values expected in the design of the model demonstrator described later in Chapter 5. In some cases, values for parameters were derived from crudely instrumented early firing tests on the demonstrator model.

The first set-up of the analog computer included the $I_P\theta$ and $I_P\phi$ terms. However, it was soon evident that these terms were very small in magnitude in most cases (and the potentiometer input settings were thus too close to zero to set in accurately). When the term was intentionally set to higher values, a very high-frequency, low amplitude motion was seen to be superimposed on the basic precessional motion of the plug, on the computer readout. It seemed obvious, after the basic dynamic equations were examined, that these terms represented the nutational motion of the plug itself.

The majority of the computer runs were made, then, with the following equations of motion (derived from Eqs. 2.18 through 2.21) approximating the plug-rocket dynamical system:

$$\ddot{\phi}_1 + \frac{K_R}{I_R}(\phi_1 - \phi_2) + \frac{K_D}{I_R}\dot{\phi}_1 - \frac{M_{\phi_1}}{I_R} = 0 \tag{3.1}$$

$$\ddot{\theta}_1 + \frac{K_R}{I_R}(\theta_1 - \theta_2) + \frac{K_D}{I_R}\dot{\theta}_1 - \frac{M_{\theta_1}}{I_R} = 0 \tag{3.2}$$

$$\dot{\theta}_2 + \frac{K_P}{H}(\phi_2 - \phi_1) = 0 \tag{3.3}$$

$$\dot{\phi}_2 - \frac{K_P}{H}(\theta_2 - \theta_1) = 0 \tag{3.4}$$

The computer set-up is shown in Fig. 4. The ranges of parameter values used in the analog simulation were:

k_R	:	0 to 45 ft-lbs/radian
k_D	:	0 to 0.2 ft-lbs/radian per second
k_P	:	0 to 7.5 ft-lbs/radian
I_R	:	1.00 slug-ft^2
I_P	:	2.33 x 10^{-4} slug-ft^2
H	:	0 to 0.366 ft-lb-sec (corresponds to 0 to 15,000 rpm)
M_ϕ	:	0 to ±0.107 ft-lbs

The analog computer study was extremely valuable in identifying critical parameters, as well as giving graphical pictures of resulting system dynamics.

3.2 Discussion of System Dynamics

The ϕ,θ plot was set up in all cases except one with an initial input angular difference between the plug and rocket axis of 0.025 radians. In order to see clearly the most general resulting motion, an initial input

tangential velocity was also inserted to result in roughly a conical motion. The typical system dynamics showed that the rocket axis tended to conically "home in" on the plug-spin axis, for reasonably small values of the parameters k_p/H and M_ϕ or M_θ. In many cases, the final orientation of both the rocket and plug axes represented a "compromise" position much closer to the original plug-spin axis than to the original rocket axis. For certain values of steady state moments, and with finite values of the parameter k_p/H, the dynamic plots revealed an interesting phenomena. The initial coning motion towards the "compromise" position was noted, but then this was followed by a slow but gradually increasing drift. For larger steady state disturbing moments coupled with larger values of the plug parameter k_p/H, this drift was quite rapid. For the more slowly drifting cases, system performance might often be considered quite satisfactory since at rocket burn-out the slow drift would not have had time to have any appreciable effect. In an actual system, initial malalignment between the plug and rocket axes would intentionally be held as close to zero as possible (by means of the alignment pin device). A number of typical systems dynamics plots are reproduced as Fig. 5(a) through (n).

3.3 Discussion of Critical Parameters

One critical parameter affecting system operation is the plug parameter K_p/H. A zero value of this parameter indicates that the plug is completely insensitive to relative motions between the plug and the rocket casing. Although practically speaking, it is impossible to obtain a zero value of K_p/H, sufficiently small values can lead to a satisfactory type of system operation typified by oscillations within specified limits of a reference axis.

Two methods for making this parameter small might be used concurrently:

a. Increase the angular momentum, H, by using a high spin rate.

b. Trim out upsetting torques arising due to modulation of the annular area.

Another critical parameter appears to be the amount of externally applied steady-state moment on the rocket body. The effect of this parameter increases with increasing values of K_p/H and is evidenced by an increasing amount of drift on the plug-spin axis.

Satisfactory system operation appears possible, provided that the combined affect of the two critical parameters described above remains within reasonable bounds. If one or the other of the parameters can be held close to zero, reasonably large values of the other parameter can be tolerated.

A useful way of looking at the critical parameters is as a system of time constants.

For a given rocket-rotating plug system, one might combine the effect of the stabilizing aerodynamic fins (if any) with the stabilizing moment effect of the plug nozzle, to give an undamped yaw/pitch time constant.

$$T_R = 2\pi \sqrt{\frac{I_R}{K_R}} \tag{3.5}$$

For the plug itself, a plug time constant is defined, representing the precessional period of the plug (due to the pressure field):

$$T_p = 2\pi \frac{H}{K_p} \tag{3.6}$$

Finally, to represent the effect of an externally applied moment, a moment time constant is defined:

$$T_M = 2\pi \sqrt{\frac{I_R}{M}} \tag{3.7}$$

Define two non-dimensional parameters, using the above three time constants:

$$\gamma = \frac{T_R}{T_P} = \frac{K_P}{H} \sqrt{\frac{I_R}{K_R}} \tag{3.8}$$

$$\mu = \frac{T_R}{T_M} = \sqrt{\frac{M}{K_R}} \tag{3.9}$$

Finally, representing the damping ratio of the rocket in pitch/yaw by means of a damping factor and the undamped pitch/yaw time constant:

$$\zeta = \frac{K_D T_R}{2} = \frac{K_D}{2} \sqrt{\frac{I_R}{K_R}} \tag{3.10}$$

The analog computer study showed that optimum performance was obtained with the values of both parameters μ and γ equal to zero. However, with either one of the two equal to zero, system operation was generally satisfactory. For the case of $\mu = 0$ (no steady-state external moment on the rocket) the value of γ could rise to 5.0. For the opposite case of $\gamma = 0$ (an insensitive plug), it was desirable to hold the value of μ to less than 0.50.

Another possibility which was investigated was that of a sign reversal on the plug parameter. Physically, this would represent a case where the pressure field would exert a moment tending to restore, or realign, the

plug with the rocket (the opposite of the predicted effect). This sign change merely changed the direction of the precession; the resulting dynamic plots were mirror images.

The effect of changing damping ratios is also clearly demonstrated in Figs. 5(a) through (n). As one would expect, a lightly damped system may in some cases be more desirable, as energy is expended more evenly in all directions around the plug spin axis. In the more heavily damped case, a great deal of the energy might be expended on one side of the plug spin axis, giving a final alignment outside of prescribed limits.

The effect of an out-of-plane moment (orthogonal to the plane of the deviation) was also investigated. Depending on the sign, such a moment resulted in a diverging or converging conical motion. For the stable (converging) motion, the plots were almost identical to those with no out-of-plane moment, but with an increased damping ratio. This effect became of some importance during the subsequent design and operation of the slotted plug described in Chapter 4.

The case represented in Fig. 5(e) is particularly significant, in that it represents a possible outer space rocket system, where no aerodynamic moments are applied ($\mu = 0$). It is noteworthy that the value of the other parameter ($\gamma = 1.49$) is more than unity.

CHAPTER 4

AERODYNAMIC PRESSURE FIELD AROUND THE ROTATING PLUG

4.1 Plug Nozzle Flow

The basic characteristics of the convergent-divergent (or Laval) type nozzle are well known. A plug nozzle may be viewed as a "modified" conventional nozzle; the basic difference being that the supersonic expansion is not confined within solid walls, but is continually redirected by ambient pressure. The gas expands inwardly as the diameter of the plug decreases and eventually acquires an essentially axial velocity vector[8].

The throat of a plug type nozzle acts no differently than the throat in a conventional nozzle. Flow is "choked" at this point, and the throat area limits the mass flow through the nozzle. One may assume a Prandtl-Meyer expansion downstream of the throat, and use the method of characteristics to compute the contour for an axisymmetrical plug which yields an ideal isentropic expansion with no disturbances in the flow.

It has been shown experimentally that simple conical-plug nozzles have the same performance trends as a contoured-plug (isentropic) nozzle. A slight decrease in the thrust coefficient of about one percent occurs with this substitution. Also, the plug angle for best performance increases from 60° to 80° as the design pressure ratio is increased from approximately 8 to 20[9].

4.2 Upsetting Moment Due to Plug-Rocket Angular Offset

For a plug nozzle in which the plug is pivoted at some internal point on the axis of symmetry of the plug the flow differences occurring due to angular offsets between the rocket and plug axes must be taken into account. These flow differences lead to a moment being exerted on the plug. Without compensation, the moment thus generated generally tends to drive the axis of a non-spinning plug further away from the rocket axis. In the case of the spinning plug, however, the moment tends to precess the plug around the rocket axis in a manner similar to the action of gravity on a spinning top.

The basic reason for the upsetting moment can best be understood by assuming all pressures upstream of the throat are equal to inlet (chamber) pressure, while all pressures downstream of the throat are equal to ambient (atmospheric) pressure. A typical calculation for the model plug showed the center of pressure to be located on the plug axis of symmetry, at 0.307" above the orifice plane. It would appear that the ideal solution to the problem would be to shift the central pivot point up to this location. Were this done, however, most of the beneficial effect of flow modulation would be lost, due to the relative tangency of the motion of the conical plug with respect to the lip of the orifice plate.

Several possible solutions to this problem were investigated. These solutions might be regarded as methods for making the plug relatively insensitive to rocket-plug angular deviations. The methods looked at involved both mechanical means, and the use of momentum exchange with high velocity gas flow past the plug. It was determined that subsonic momentum exchange upstream of the throat yielded insignificant trim moments. However, the use of

vanes or slots in the sonic and supersonic regions at and downstream of the throat area did yield significant compensatory moments. Also, a flexural joint support for the plug capable of yielding a centering moment was investigated, and was found to have sufficient cross-section to withstand the axial loads of thrusting.

In designing turning slots, or vanes, for the plug, three goals were considered desirable (see Fig. 6):

a. Maintaining the spin rate.

b. Exerting a trimming moment partially or completely countering the upsetting moment described previously.

c. Exerting a small out of plane moment giving the plug a slight tendency to precess toward the rocket axis.

The effect of the moment described in (c) above would then ensure a stable tendency for the system where steady-state moments exerted on the rocket body would result in a low rate drift of the plug spin axis, but would delay the plug's contacting its mechanical limit stops.

CHAPTER 5

MODEL DESIGN AND CONSTRUCTION

5.1 Design Philosophy

The design and construction of a small working model of the rotating plug concept proved typical of most research projects. That is, some anticipated problem areas gave no trouble whatsoever (example: static and dynamic balancing of the plug was not even necessary due to symmetrical design and manufacture); while other areas in which little trouble was expected gave more than their share of problems (example: ducting high pressure air through a flexible joint).

In the design and construction of the model, simplicity was the keynote. Easily available and inexpensive mechanical components were used wherever possible. Where specially designed major components (such as the plug itself) were required the simplest design possible was chosen. In two key locations, the use of circular retainer rings (TRUARC type) led to a simple design and rapid assembly of the system. The plug nozzle is shown assembled and disassembled in Figs. 7 and 8.

Early construction and testing of a rotating plug model, capable of being tested under either spinning or non-spinning conditions, gave a degree of confidence in the basic assumptions and theory. It also led to timely redirection of study efforts in the proper paths.

5.2 Design of Rotating Plugs

A number of possible ways of supporting the rotating plug were considered, including:

a. Spherical air bearing
b. Angular contact ball bearing mounted outboard of universal joint
c. Self-aligning aircraft type bearing

After considering the cost factor, approach (a) was ruled out. Then, six tentative designs using approaches (b) and (c) were drawn. The final choice involved using approach (c) with the smallest commercially available self-aligning bearing (SHAFER type A-4). The limits of angular deviation of this bearing were ±10°. This type of bearing is normally used in aircraft control rod ends at low cyclic rates.

The plug itself was designed to operate up to chamber pressures of 100 psig, using compressed air. This resulted in a pressure ratio of approximately 7. A simple conical plug shape was selected with a plug angle of 60°, close to optimum for this pressure ratio[10]. Some adjustment of the central pivot point was contemplated, so the bearing was retained within the cone using shims of varying thicknesses in pairs. The shims contacted the bearing outer race, and the upper shim was held by a circular retainer snap-ring.

Two plugs were constructed. Plug #1 had smooth sides, while Plug #2 contained spin-up slots in the annulus region (see Fig. 9). Otherwise, they were completely interchangeable. Basic features of plug design are shown in Figs. 10 and 11.

Initial spin-up for both plugs was accomplished through a recessed hexagonal fitting at the cone vertex. An Allen-type fitting was driven by either an electric

or air drill after insertion in the plug fitting. The turning slots machined into the sides of Plug #2 served to maintain (or increase) the spin rate, and also to provide a slight trimming moment as shown in Fig. 6.

Limit stops for the plug were provided by designing the cage to contact the shoulder of the plug at angular deviations of ±8°, since the limits on the A-4 bearing were ±10°. Also, three set screws were provided allowing non-spinning tests at any fixed angles up to ±8°.

5.3 Design of Ducting

The three major components which control the ducting of the compressed air past the rotating plug are designed for quick assembly using a 4.5" dia. snap-on type retainer ring. The three components were named cage, casing and orifice plate to indicate their function (see Figs. 12 through 14). The similarity of the model plug-nozzle ducting system to the 1954 NACA models[9] was intentional. Specific design features were determined on the basis of a 60° plug angle and an outer shell angle of 45°[10].

The shroud surrounding the plug was machined into the cage to keep foreign matter from passing through the bearing. This was considered necessary as the normal bearing seals had been removed to reduce friction.

5.4 Design of the Test Rig

The entire test rig was located in the compressor room at the MIT Aerophysics Laboratory. Compressed air was supplied to the nozzle by two Chicago Air Compressors, Type 16-14" x 14" O-CEO, with a combined steady-state output of 1.7 lb/sec. The compressed air was controlled through a quick-acting, manually operated gate valve, with

a finite number of adjustable limit stops. The air was then directed vertically downward through a 2" pipe to a Flexpipe flexible bellows, type 2M10Z. A short length of 2" aluminum pipe was attached to the lower end of the Flexpipe, terminating in the nozzle assembly. The length of this pendulous portion was 49", measured from the center of the Flexpipe. Surrounding the pendulous portion of pipe was a steel safety hoop which allowed a maximum pipe deflection of 13 1/2° from the vertical (see Fig. 15).

CHAPTER 6

INSTRUMENTATION

6.1 Measured Parameters

The following parameters were measured directly on the final test series by the means indicated:

Plug Angle	photocell	Sanborn Recorder Ch. 3
Plug Angle	photocell	Sanborn Recorder Ch. 4
Plug rpm	photocell	Sanborn Recorder Ch. 2
Pipe (rocket) Angle	electr. pot.	Sanborn Recorder Ch. 5
Pipe (rocket) Angle	electr. pot.	Sanborn Recorder Ch. 6
Chamber Pressure	transducer	Sanborn Recorder Ch. 1

6.2 Measurement Circuitry

All three plug parameters were measured by a system of cadmium sulfide photoconductor cells scanning a black and white harlequin pattern painted on the plug. Aluminum instrumentation cubes (1" x 1" x 2-1/2") were fabricated to hold the photocells and 20.1 mm focal length double convex lenses with provisions for focussing. Illumination was provided by a 6-volt lamp mounted on each cube. The two orthogonal plug angles, $(\phi_2-\phi_1)$ and $(\theta_2-\theta_1)$, were measured by the two outer photocell cubes scanning a horizontal black-white interface on the plug. Plug rpm, $\dot{\psi}_2$, was measured by the center photocell cube scanning a vertical black-white interface on the plug. (See Figs. 16 and 17.)

The rpm circuit diagram is shown in Fig. 18. The rpm envelope circuit (output BNC #2) did not provide adequate data and was not used. Data on rpm was obtained by direct pulse count readout from BNC #1.

The plug angle measurement system is shown in Fig. 19.

The two pipe (rocket) angles were measured by means of orthogonally mounted linkages connected to 1K helipots and powered by 1-1/2 volt dry cells.

The electrical diaphragm type pressure transducer had a range of 14.7 to 100 psia. The pressure tap was located in the casing, 1-1/2" above the orifice plane. A back-up, direct reading Bourdon-type gage was also located at this position for the convenience of the test conductor.

The assembled instrumentation is shown mounted on the casing in Fig. 20. The pressure transducer power supply and angle/rpm circuit boxes are shown in Fig. 21.

6.3 Calibration of Instrumentation

The calibration methods employed in the course of final phase testing were relatively straightforward:

a. RPM calibration was not necessary, as pulse counts per unit time were read directly from Sanborn Recorder tapes.

b. The pressure transducer/power supply system was calibrated once, using an accurate pressure source. A calibration curve was made up, and used for all subsequent tests. Output was in millivolts and had excellent linearity. Sensitivity was 0.185 mv/psi.

c. Plug angles were calibrated only at the plug limit stop angles prior to each series of runs. This was accomplished by wobbling the cone around in contact with the cage, with the photocell system active.

d. Pipe angles were calibrated before each run, by running the pipe manually against the safety hoop limit stop in each of the four quadrants.

It is possible that the photocell readout of plug angles was not too linear. Angular motions could produce deviations

in light intensity and also affect focussing. The traces on the Sanborn tape appeared very sinusoidal and regular, however.

Pipe angle linearity was probably affected by some cross-coupling between the linkages connecting the pipe to the two helipots. Although the linkages appeared crude, they functioned smoothly and reliably. Their mass was almost negligible, compared with that of the heavy nozzle assembly components.

CHAPTER 7

TEST RESULTS

7.1 General Outline of Tests

The initial test phase was conducted when only the smooth-sided plug (Plug #1) was available. The instrumentation package was still in the design and construction process; as a result, the first test phase yielded only qualitative information, or at best crude measurements of some of the basic parameters. The early initiation of testing was very valuable, however, in the following respects:

a. It determined important features of the system to consider in further design, construction, and testing.
b. It established test procedures and trained test personnel.
c. It ironed out initial hardware-type problems.

The second and final test phase used both Plug #1 and Plug #2. In addition, full instrumentation was available, and resulted in a great deal more quantitative data.

7.2 Spin-Down Tests

Initial spin-down tests were conducted using a photocell counter and an EPUT meter. The bearing was unloaded (no air pressure on the plug). A primary goal of this early test was to determine the suitability of a self-aligning type bearing at high rpm's for short time periods.

Results were highly satisfactory, in that a large number of runs up to the vicinity of 16,000 rpm showed no sign of overheating or bearing deterioration. Although several different types of bearing lubricants were tested, little difference was noted. A breakdown between bearing friction and windage was not attempted. Results of a typical spin-down test are given in Fig. 22.

7.3 Side Force Measurements

The first thrusting tests were made with the plug restrained by set screws within the casing, (plug not spinning). Side forces were measured using a fish scale, ensuring that the pipe was vertical so that a weight component would not be measured. Plug-rocket angular deviation was calculated from measurements of the orifice gap at four locations 90° apart. The orifice gap measurements also gave the throat area, from which thrust could be calculated. These tests successfully demonstrated that a corrective side force on the rocket was generated by the offset plug. The results of one series of side-force tests are given in Fig. 23.

7.4 Preliminary Free-Spin Tests, Plug #1

The first thrusting, free spin, tests on Plug #1 were conducted with extremely limited instrumentation. Chamber pressure was read manually from the Bourdon pressure gage mounted on the casing. RPM was measured using a photocell scanner and EPUT meter. Angles were visually estimated by the test conductor. The general impression of the tests was that the plug and pipe appeared stable at high rpm's; but that at lower rpm's the plug began a diverging precessional mode. This motion would eventually drive both the plug and the pipe

against their respective limit stops. The pipe would then remain forced against the limit stop by the side force generated by the (now stationary) plug. Qualitative test results of Phase 1 Free Spin Tests on Plug #1 are presented in Table 7-I. The increase in initial rpm from 16,000 to 18,000 was obtained through switching from a small electric drill to an air-driven drill.

TABLE 7-I

PRELIMINARY FREE SPIN TESTS, PLUG #1

Run No.	Initial RPM	P_c psig	Initial Plug Angular Offset (deg)	Running Time (sec)	Remarks
1	16,000	32	0	5	Plug stable first 3-4 sec, then precessional divergence of increasing frequency noted as plug slowed. After contacting plug limit stop, pressure flow held plug in this position. Pipe limit not reached.
2	16,000	37	3	5	Plug stable first 3 sec, pipe began moving immediately in correct direction to realign with plug spin axis, then began to diverge spirally. Plug and pipe hit limit stops.

TABLE 7-I (Continued)

Run No.	Initial RPM	P_c psig	Initial Plug Angular Offset (deg)	Running Time (sec)	Remarks
3	16,000	36	3	5	Plug appeared stable at first. Pipe moved toward plug spin axis, then moved off roughly 90° from initial motion. Plug and pipe hit limit stops
4	18,000	33	0	5	Plug and pipe appeared stable for about 3 sec, then began slowly divergent conical precession

Note: Limited Instrumentation Available; all figures except P_c approximate.

7.5 Final Series Free-Spin Tests

The final series of free spin tests on both plugs were conducted using full instrumentation. A total of 15 thrusting runs were made, and runs were terminated at the failure of the second A-4 bearing.

Free spin tests using Plug #1 revealed an interesting phenomena. An initial conical precession mode occurred on the first run, probably due to the initial malalignment between the pipe and the plug. During spin-down from 18,000 rpm to about 10,000 rpm, this precession tended to damp out. However, as the plug continued to slow down, the amplitude of this precession stabilized and then began to increase until the plug contacted the mechanical stops (see Figs. 24 and 25).

As the chamber pressure was increased in succeeding runs the plug precession period decreased. The time required for the plug to contact the limit stops also decreased.

On Run no. 9, Plug #2 was substituted for Plug #1, and the pipe was restrained. A low value of chamber pressure was used initially, and even this was applied gradually. The plug began to diverge almost immediately in its precession, and had contacted the stops before the full chamber pressure was even reached. The mechanical limit stops were contacted at approximately 1.0 sec.

Run no. 10 was somewhat longer, about 2.4 sec, before contacting the limit stops. On this run, the pressure was applied so gradually that not even half pressure had been applied at the time of contacting the stops. Initial spin-up had been 16,500 rpm, and it was noted on this run that the turning slots had been effective in increasing the spin rate of the plug. By the time the limit stops had been contacted, plug rpm was at 19,200.

Run no. 11 was similar to the previous runs, as regards the gradual pressure buildup. Again, the plug contacted the limit stops following a conical divergence. At this point, it was surmised that the gradual application of chamber pressure was possibly having an undesirable effect in acting only on the upper portion of the slots, giving an unstable value of M_c. Accordingly, instructions were given to apply full pressure immediately, so that the pressure would in fact have its point of application farther down on the slots and possibly change the sign of M_c.

Run no. 12 appeared to confirm the hypothesis of the previous paragraph. The initial spin-up rpm was 15,600. Upon application of full chamber pressure of 67.3 psig

which occurred with 0.25 sec, the initial conical motion due to plug malalignment began to decrease in amplitude, and by t = 1.7 sec had effectively died out. The pipe stabilized sooner than the plug and picked up a bias angle off the vertical (see Fig. 26). (Only ϕ angles have been plotted, as θ values were similar.) At the same time, between t = 0 and t = 2.8 sec, the slots had accelerated the plug to 27,600 rpm. At this point, bearing failure began, and after a slight wobble in plug angle, the plug came to a dead stop in roughly the centered position.

Following disassembly, the bearing was found to have catastrophically failed, with the roller retainers ground to fine particles and lying in the plug cavity. All the conical rollers were jammed together on one side of the bearing, and effects of excessive heating were evident.

The second bearing was installed, and a new lubricant was used. This was Dow-Corning Type 33 silicone grease, medium consistency, operating temperature 100-300°F, maximum speed factor 150,000 to 200,000.

The first run with the new bearing (Run no. 13) was made, reverting to the gradual application of pressure. The run was similar to the previous unstable ones, in that divergence was rapid, and limit stops were contacted before full pressure had been reached.

Run no. 14 was made, this time using a rapid application of chamber pressure, (P_c of 64.8 psig was reached within 0.20 sec. (see Fig. 27). The conical precession of the plug began to damp out immediately. The test conductor struck the pipe sharply (intentionally) during the first 0.1 sec of pressure application, to check system response. The pipe resisted this force and appeared to remain stable; this fact was later confirmed by analyzing the Sanborn traces. The plug continued to accelerate on this run, due to the effect of the turning slots. By

t = 1.4 sec, both pipe and plug angles were stable, and rpm had reached 40,100. The plug continued to accelerate until at t = 2.3 sec the air valve was closed. Pressure then tailed off to atmospheric in about 0.3 sec, and the measured peak rpm value was 50,300 rpm. At the time of the test, the Sanborn traces were not analyzed, and it was not realized that this high an rpm value had been attained, although it was known that the plug had accelerated to a value higher than the initial spin-up attained with the air drill external drive.

Since no apparent damage had occurred to the bearing, Run no. 15 was made. This time, the test conductor struck the pipe twice following application of air pressure. The pipe resisted both impacts, with no noticeable deviation on the Sanborn traces. On this run, the plug stabilized more quickly, due to a smaller initial malalignment. Again, acceleration was rapid, and peak rpm of 42,000 was reached at t = 2.0 sec. However, slightly before this, the incipient bearing failure was evident in several jerky excursions in the plug angles traces, beginning at t = 1.7 sec. The bearing came to a complete stop by t = 4.5 sec, in a manner identical with Run no. 12. The period of time during which the pipe angle was stabilized by the nozzle at a bias angle off the vertical was thus shorter than noted in Run no. 14; otherwise the plots were very similar.

It is interesting to note that on Runs 12,14, and 15, the nozzle was successful in stabilizing the pipe at a position which was biased off the vertical. In Run 14, for example, the pipe angle was constant from t = 1.0 sec to t = 2.25 sec. In Run 12, pipe angle was virtually constant from t = 1.25 sec to t = 3.00 sec. It is in this region of high plug rpm that performance is shown to be optimized.

A final run (Run no. 16) was made to measure the natural (pendulous) frequency of the pipe and nozzle assembly complete with all instrumentation attached. A period of 2.00 sec was measured.

7.6 Determination of K_p from Experimental Results

From the Sanborn traces, the period of plug precession, T_p, could be measured under a variety of conditions. Knowing this parameter and the rpm, K_p could be derived from Eqs. (3.6); i.e.,

$$K_p = \frac{2\pi H}{T_p} \tag{7.1}$$

It was assumed for purposes of this study that the value of K_p is roughly proportional to the gage chamber pressure. All values were then reduced to a standard chamber pressure of 64 psig (the value obtained in Run no. 14). Derived K_p values are given in Table 7-II. A number of possible reasons for the rather wide scatter were explored. Aside from non-linearities which are bound to exist, two significant factors were noted. The first was the fact that some data points were taken as the chamber pressure was building up towards its maximum value and thus do not represent steady-state conditions. The second factor involves data points involving significantly large plug angular deviations (>2°).

TABLE 7-II

K_P AND $K_{P_{std}}$ DERIVED FROM MEASURED VALUES OF T_P

Run No.	Plug No.	RPM (meas)	Hx10^4 ftlbsec	$T_{P_{meas}}$ sec	P_C psig	K_P ft.lb/rad	$K_{P_{std}}$ ft.lb/rad	Notes
2	1	17300	.424	0.240	56.3	11.10	12.6	(2)
4	1	10200	.249	1.040	8.3	1.51	11.6	
6	1	16800	.410	0.480	14.3	5.36	24.0	(1)(2)
6	1	16200	.396	0.236	41.8	10.53	16.1	(1)(2)
6	1	15000	.366	0.352	33.3	6.52	12.60	(1)(2)
8	1	16800	.410	0.507	19.3	5.08	16.8	(1)(2)
8	1	12000	.293	0.376	21.3	4.90	14.7	(2)
9	2	17400	.419	0.628	21.3	4.19	12.6	(2)
12	2	15600	.376	0.170	67.3	13.9	13.2	
12	2	40800	.981	0.344	67.3	17.9	17.1	
14	2	24000	.577	0.176	64.0	20.6	20.6	(2)
14	2	40200	.967	0.340	64.0	17.9	17.9	
14	2	48600	.470	0.470	64.0	15.7	15.7	
15	2	29400	.708	0.284	66.3	15.7	15.1	

Notes: (1) Measured with P_C increasing

(2) Measured with $|\theta_2-\theta_1|_{max} > 2°$

7.7 Critical Frequencies of Spinning Tops and Spinning Plugs

Experiments on the smooth sided plug and the pipe vertically restrained showed an interesting parallel to the theory of the "sleeping top". Pressure forces on the plug in this case act in a manner analogous to gravity acting on a top. That is, an upsetting moment is felt by the spinning body as its axis deviates from the vertical. A

"sleeping" top tends to rise by itself towards the vertical, provided it has enough angular velocity. The critical angular velocity relation for a top is given as follows[11]:

$$\omega^2 C^2 > 4WA\ell \tag{7.2}$$

where A is the transverse moment of inertia
C is the spin moment of inertia
W is the weight
ℓ is the distance from vertex to c.g.

It can be seen that $W\ell\theta$ represents the moment which is applied by gravity at small angles; for the plug this moment would be written $K_p\theta$. It would appear that a direct substitution of K_p for $W\ell$ in Eq. (7.2) would give the critical angular velocity for the rotating plug. The gradual spin-down of the smooth plug in Runs no. 4 and 5 permitted the measurement of rpm at the point of divergence of the plug axis. For Run no. 4, and taking the computed value of K_p, the critical angular velocity is computed to be:

$$\omega > \sqrt{\frac{4 K_p A}{C^2}} \tag{7.3}$$

which gives:

$$\omega > \sqrt{\frac{4(1.51)(2.01)}{(2.33)^2 \ 10^{-4}}}$$

$$\omega > 149.4 \text{ RAD/SEC} = 1430 \text{ RPM}$$

But, the observed value at which the plug appeared critical was 9000 rpm (see Fig. 24).

The explanation for this discrepancy is not fully understood at the time of writing. One possibility involves

the generation of a moment on the plug opposite to M_C in Fig. 6, by exhaust gases which are dragged around with the rotating plug. Such a moment might explain the apparent increase in critical frequency, due to its destabilizing effect.

It is of considerable interest to determine what values of the critical parameters were obtained in the model tests. The value of μ was essentially zero, since all tests started at, or very close to, the vertical axis. Hence, there were no strong pendulous moments to overcome. Even so, the value of the other parameter, γ, was much higher than would be expected in an actual vehicle system, due to the high mass and inertia of the pipe, nozzle assembly and instrumentation. However, during the high rpm phase of Run 14, the computed value of γ range from approximately 4.25 down to 2.85. This set of parameter values matches closely the analog computer case shown in Fig. 5(j). This set of dynamics appears quite stable, although the final alignment of the pipe lies closer to the initial alignment of the pipe rather than the initial alignment of the plug. This appears to be the penalty paid for a value of γ greater than unity. Even so, in practice this might not be too serious, since it is assumed that both the rocket and the plug would be lined up initially, and this position would represent the final alignment position as well.

7.8 Estimation of Model Plug Equilibrium RPM

Manglesdorf's Method[12] was used to estimate the equilibrium for model Plug #2, using rpm data obtained from Run no. 14. The equilibrium rpm is estimated to be approximately 55,000 rpm, limited by bearing friction (see Fig. 28). The design of the turning slots was overly

pessimistic; the slots appeared to be much more effective than anticipated. It had been feared that most of the flow would pass by the indented slot area, reducing effectiveness. In fact, it appeared that the pressure gradient had forced air into the slots, at the same time accelerating the flow and increasing the net effectiveness in spinning up the plug.

CHAPTER 8

CONCLUSIONS AND RECOMMENDATIONS

8.1 Conclusions

In a rotating plug nozzle:

a. assuming an inertially stiff plug, annular throat modulation of exhaust gases yields a corrective moment around the rocket vehicle c.g.

b. the plug demonstrates a precessional divergence below a certain critical rpm, which is greater than that predicted by the theory of the "sleeping" top.

c. at rpm's above critical, the rotating plug nozzle can act as a filter to damp out pitch and yaw motions of the rocket.

d. the critical parameters can be defined as a system of time constants, given in Chapter 3.

e. isolation of the bearing from the main exhaust stream is possible.

In view of the fact that stable operation of a rotating plug nozzle system has been experimentally demonstrated, the broad goal of this research effort has been achieved.

It is recognized that the basic problems associated with fixed plug nozzles will remain with rotating plug nozzles. Most serious is the problem of throat erosion with high temperature gas flow. It is concluded that the ultimate success for a rotating plug nozzle system is tied closely to successful operation of fixed plug nozzles. Once the fixed type gains acceptance, the rotating type could

probably be developed with a moderate additional research effort.

It is possible that early use of the rotating plug nozzle might be contemplated in space research vehicles, since there should be no significant external moments applied in outer space; thus, the value of the parameter μ should remain near zero.

The bearing failures should not be considered too seriously. They were anticipated, as the normal operating limits of the bearings were being far exceeded. The important conclusion to be drawn is that a successful attitude stabilization for a few seconds was accomplished with a rapidly spinning plug nozzle. This probably marks the first successful demonstration of a spin stabilized nozzle (on a non-spinning rocket; pipe, in this case).

8.2 Recommendations

In view of the successful theoretical and experimental research on the rotating plug represented by this study, and possible widespread future operational uses in rocketry, continuation of this area of research is recommended.

More specifically, it is recommended that:

a. further analytical study be undertaken to gain a better understanding of the pressure flow field around the spinning plug, and the prediction of out-of-plane moment components.

b. the use of air bearings for operation of test models at much higher rpms and for longer periods of time be investigated.

c. mechanical methods of achieving trimming moments (flexural joint), with the goal of near-zero values of K_p be investigated.

d. instrumentation sensitivity and linearity be improved upon in future test models. Theoretically it should be possible to add voltages representing

say, θ_1 and $(\theta_2-\theta_1)$ to obtain θ_2 (plug inertial angle) directly.

e. a cold gas or steam version of the present test article be given a free flight test. This could be done cheaply.

f. an attempt should be made to spin up the plug from 0 rpm using main exhaust gas. The centering torque due to forces in the slots should aid in precessing the plug to the pipe axis (the pipe should stabilize the plug), until a region of low γ is reached. Then, the roles should be reversed, and the plug should stabilize the pipe.

APPENDIX A

MASS AND MOMENT OF INERTIA DATA

Item	Wt. (lbs)	I_{spin} (slug ft^2)	I_{transv} (slug ft^2)
Plug #1 (smooth sides)	1.1951	2.33×10^{-4}	2.01×10^{-4}
Plug #2 (with turning slots)	1.2150	2.30×10^{-4}	2.01×10^{-4}
Orifice Plate with O-ring	1.2987		
Cage with set screws	1.1179		
Housing	3.7000		
Photocell Package	1.2635		
Large Retainer Ring	0.1058		
Small Retainer Ring	0.0046		
Bolt, Brass Shim, Washer, Nut	0.0778		
Shims (pair)	0.0036		
A-4 Bearing (seals stripped)	0.1837		
Pressure Transducer	0.1036		
Pressure Gage	0.5821		

Note 1: I_{spin} includes bearing outer race and shims
Note 2: Pivot point 0.39 in from plug upper surface
Note 3: Center of gravity 0.65 in from plug upper surface

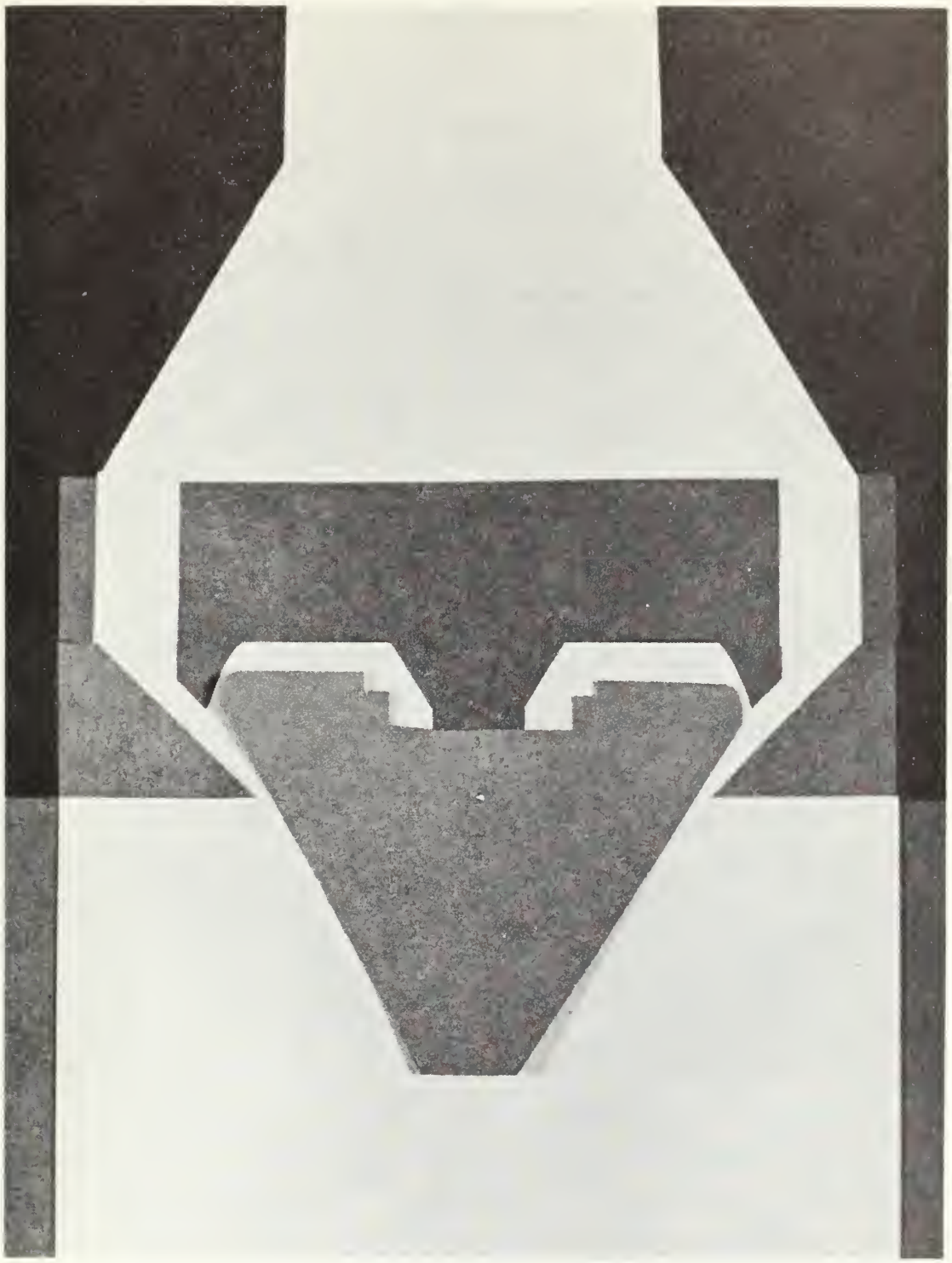

Figure 1. Rotating plug nozzle - schematic

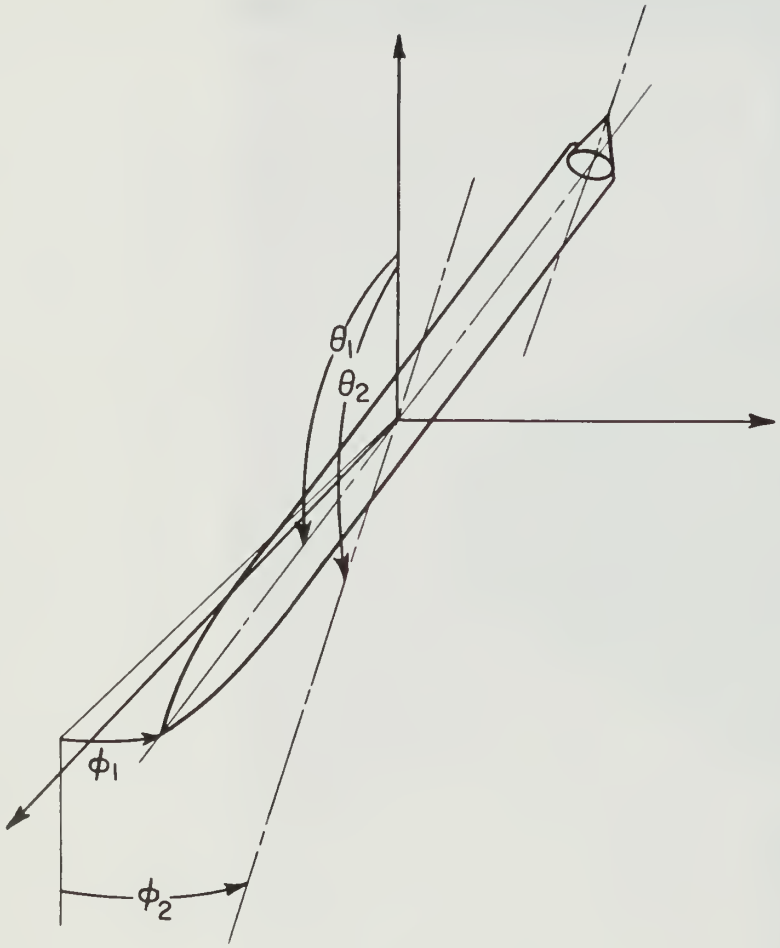

Figure 2. Rocket-plug coordinate system

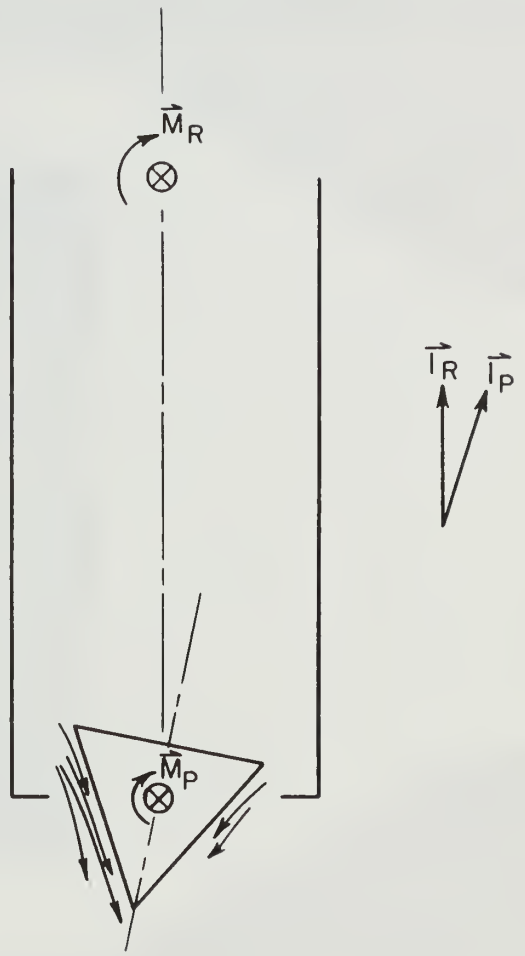

Figure 3. $\vec{M}_R$ and $\vec{M}_P$ vector moment representation

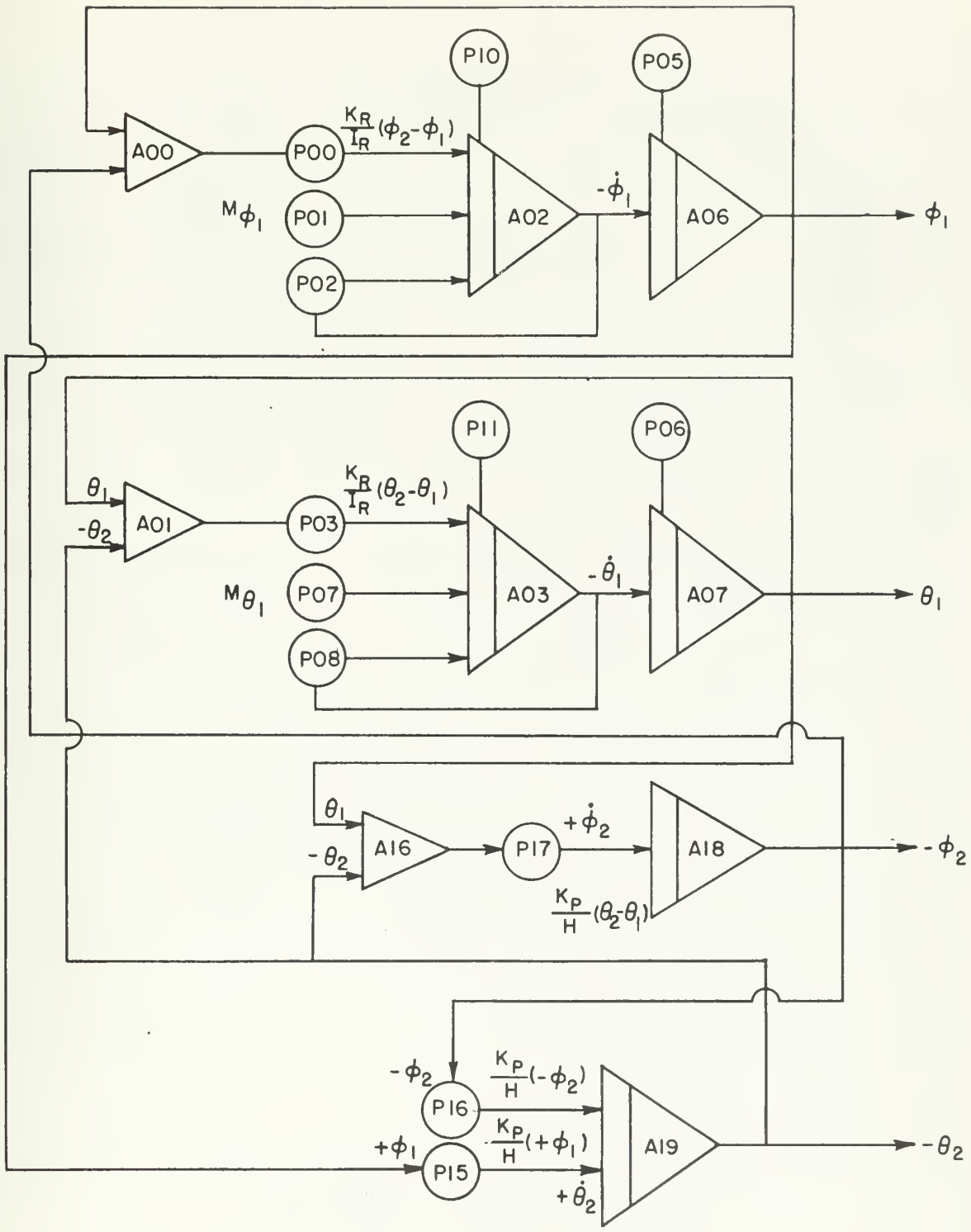

Figure 4. Analog computer set-up: rotating plug nozzle

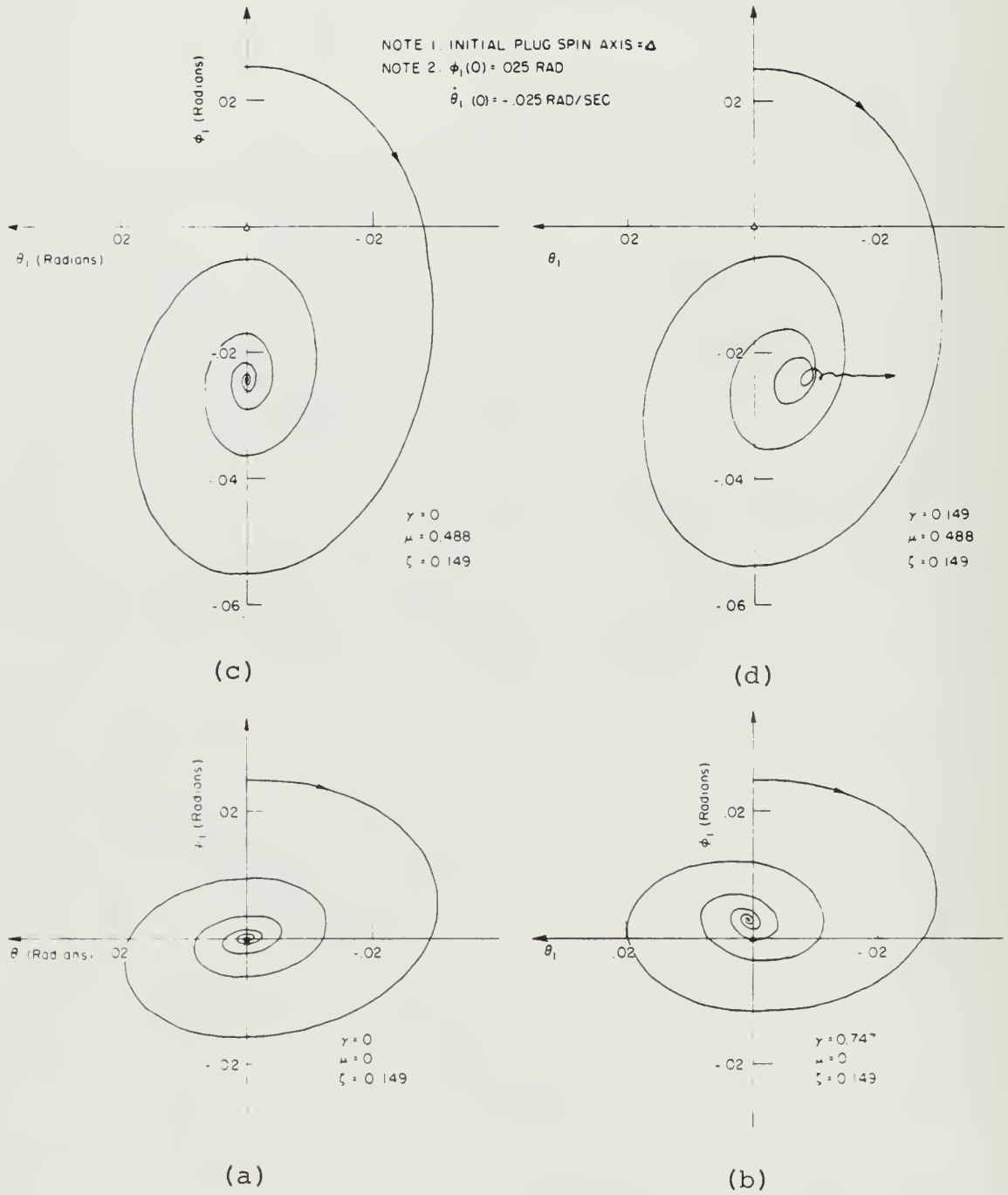

Figure 5. Rocket angle plots
$\phi_1(0) = 0.025$ rad
$\dot{\theta}_1(0) = 0.025$ rad/sec

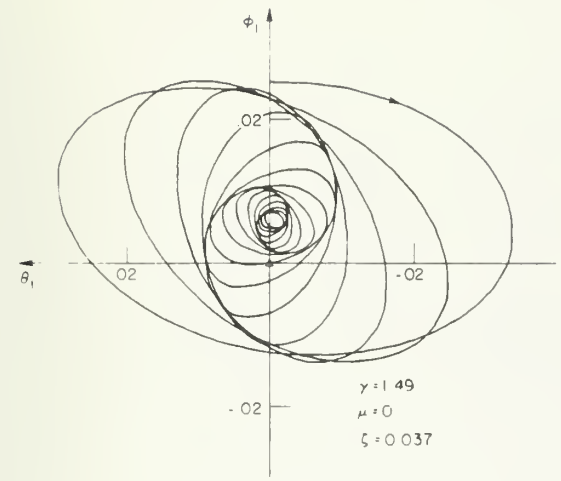

(e)

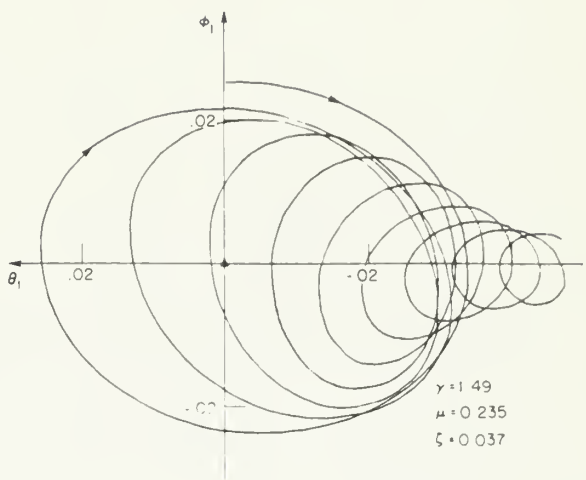

(f)

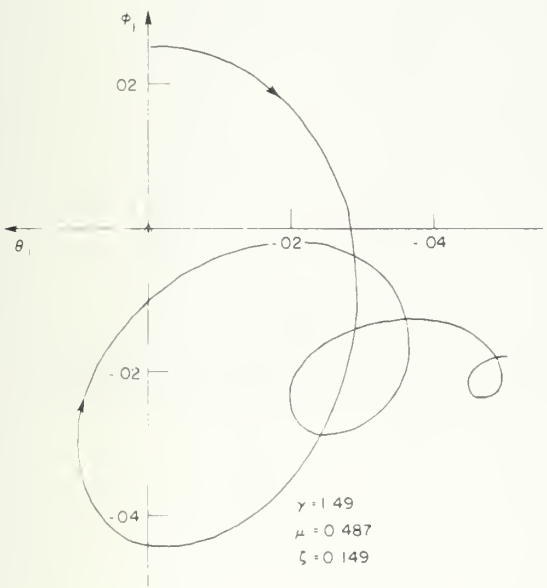

(g)

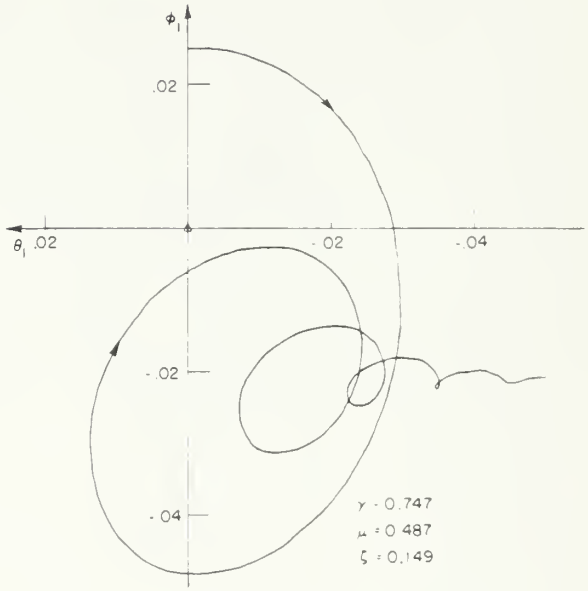

(h)

Figure 5. Continued

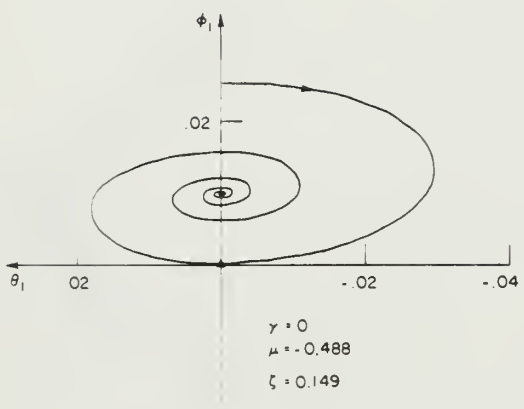

(i)

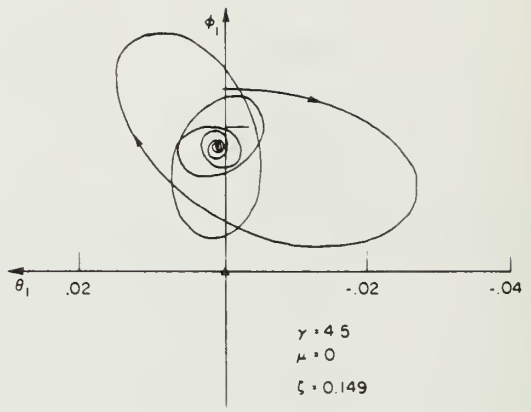

(j)

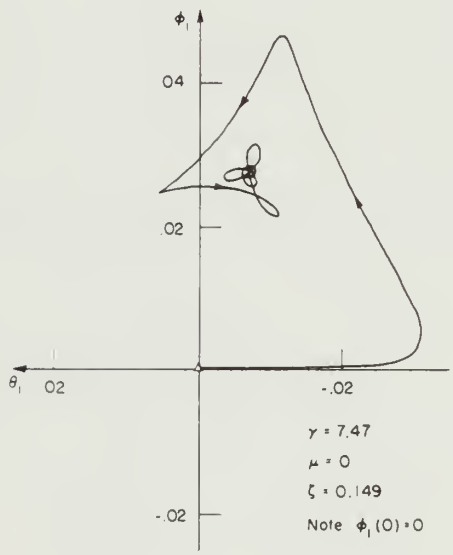

(k)

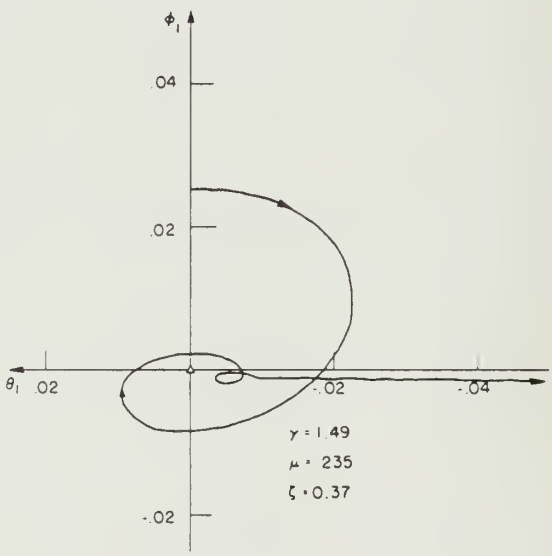

(l)

Figure 5. Continued

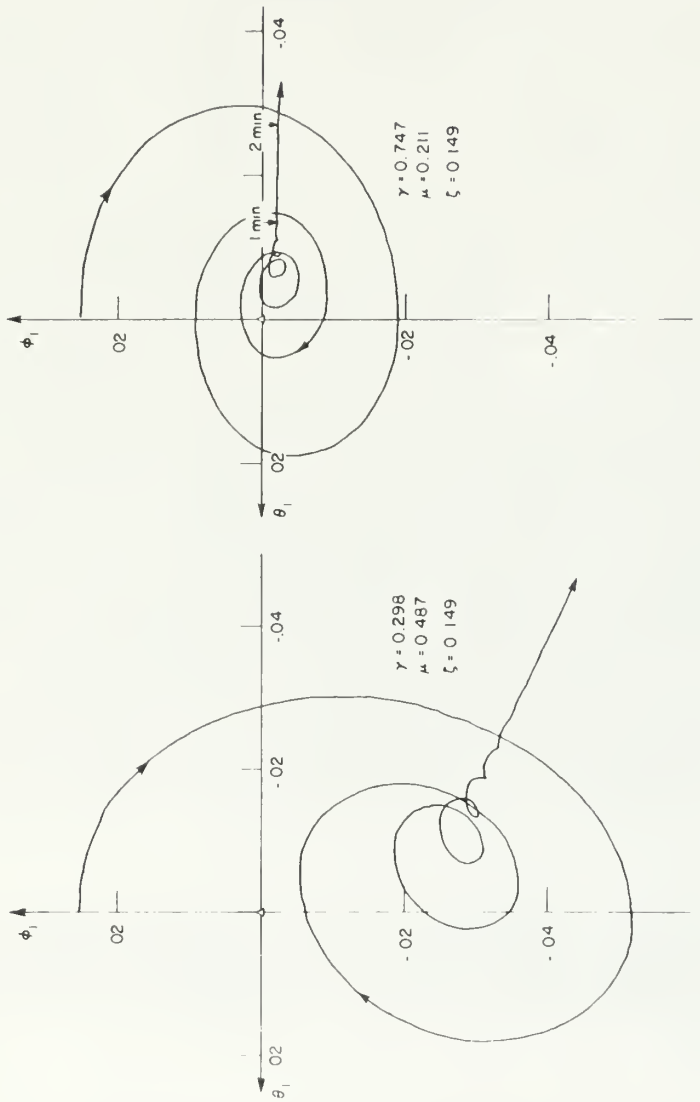

Figure 5. Concluded

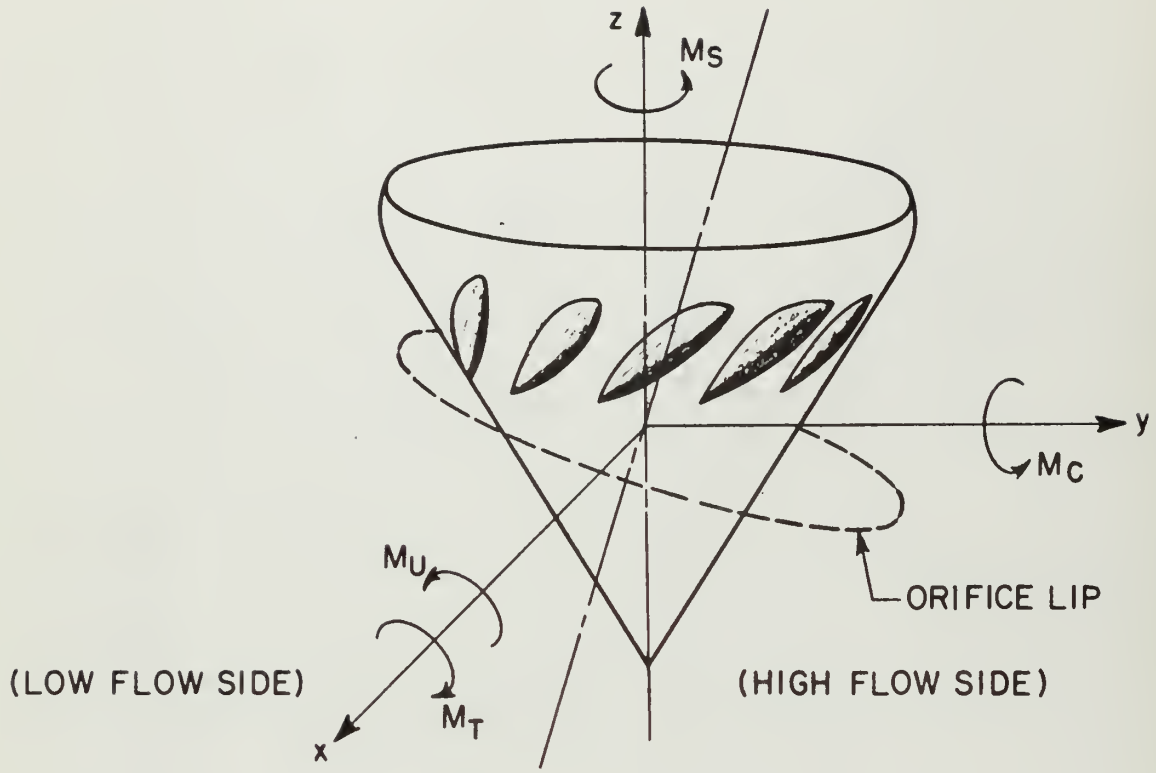

Figure 6. Rocket rotated around x-axis, showing various moments

M_u = upsetting moment

M_T = trimming moment

M_s = spinning moment

M_C = centering moment

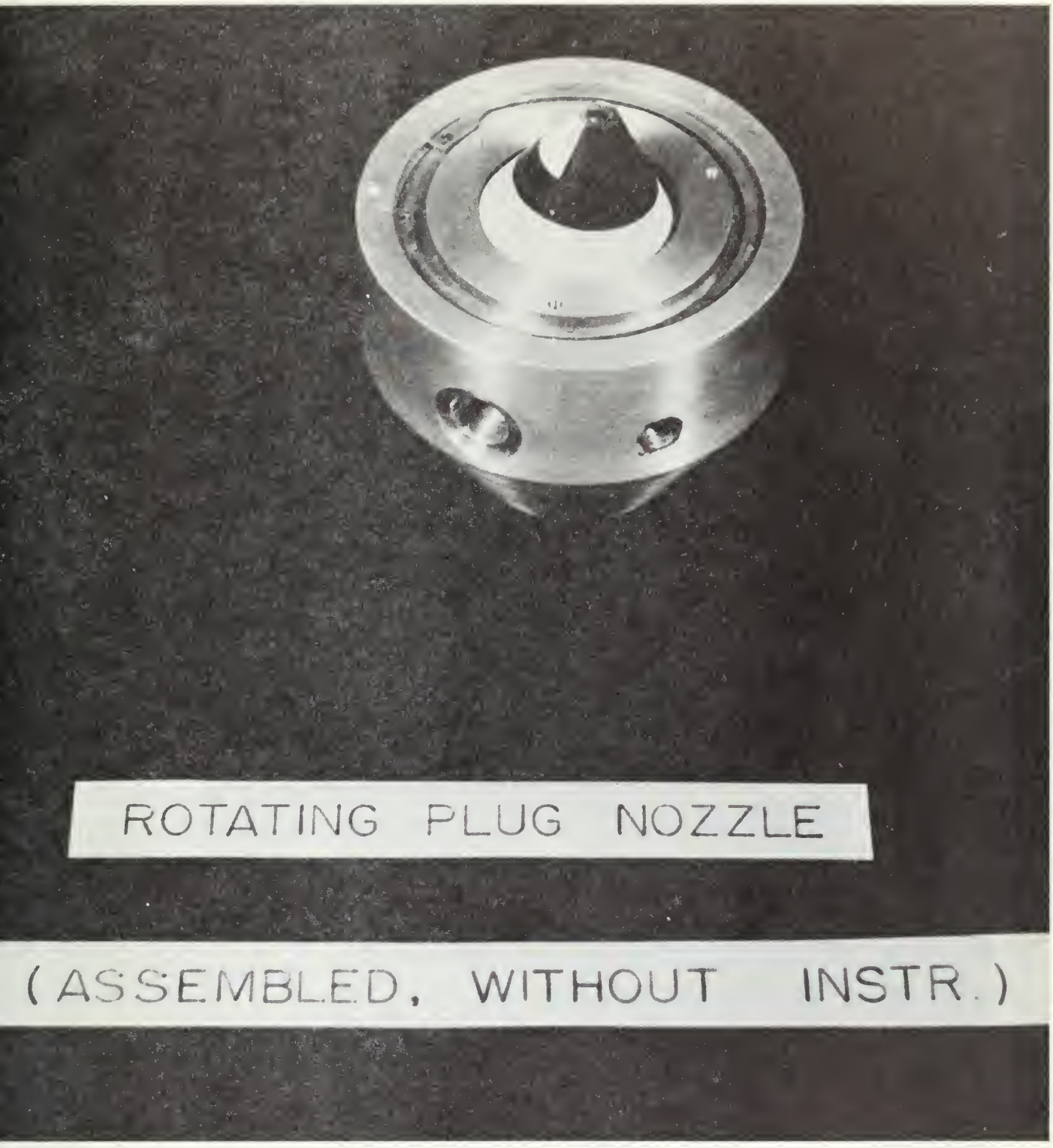

Figure 7. Plug nozzle, assembled

Figure 8. Plug nozzle, disassembled

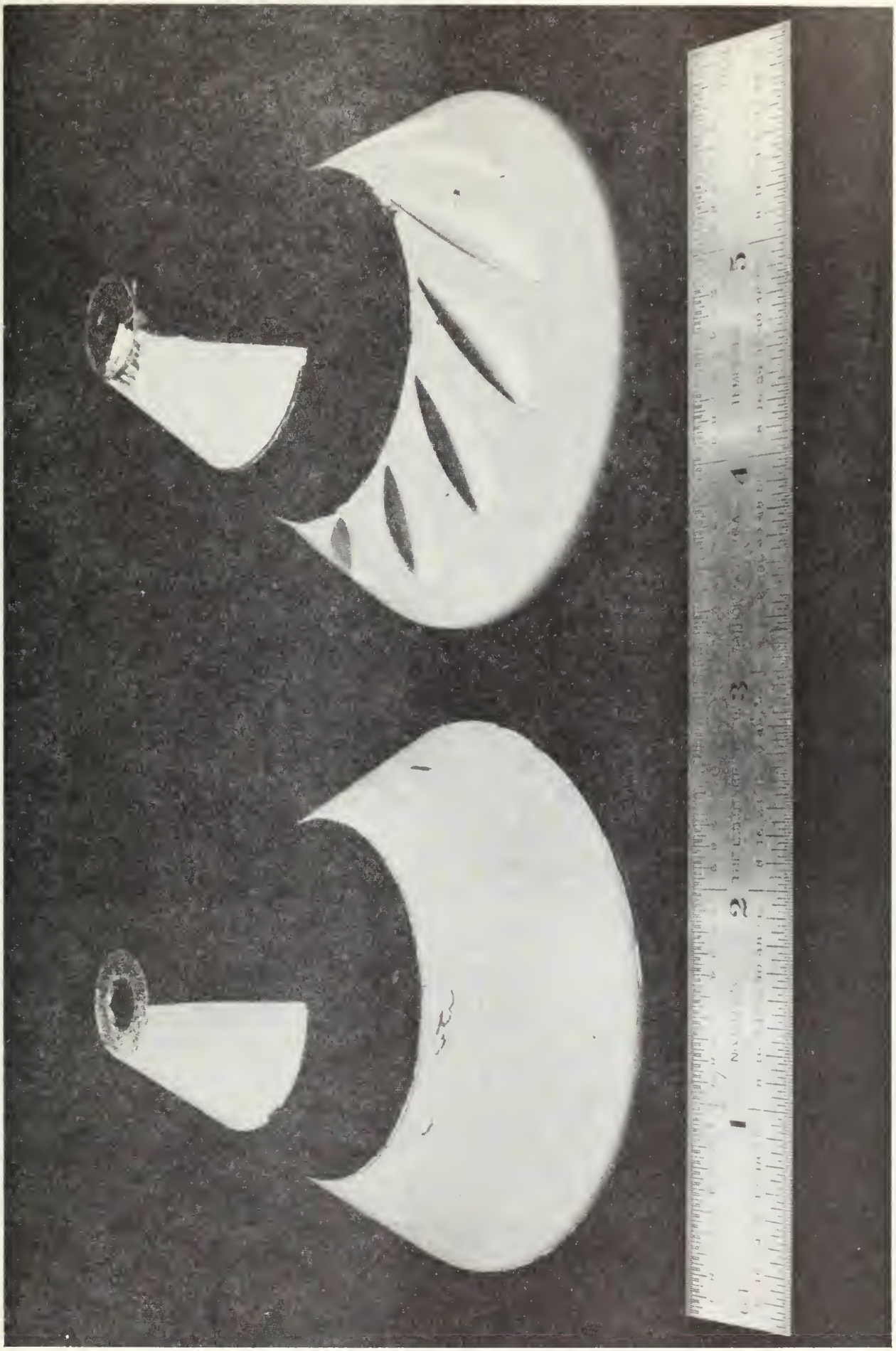

Figure 9. Plug #1 and Plug #2

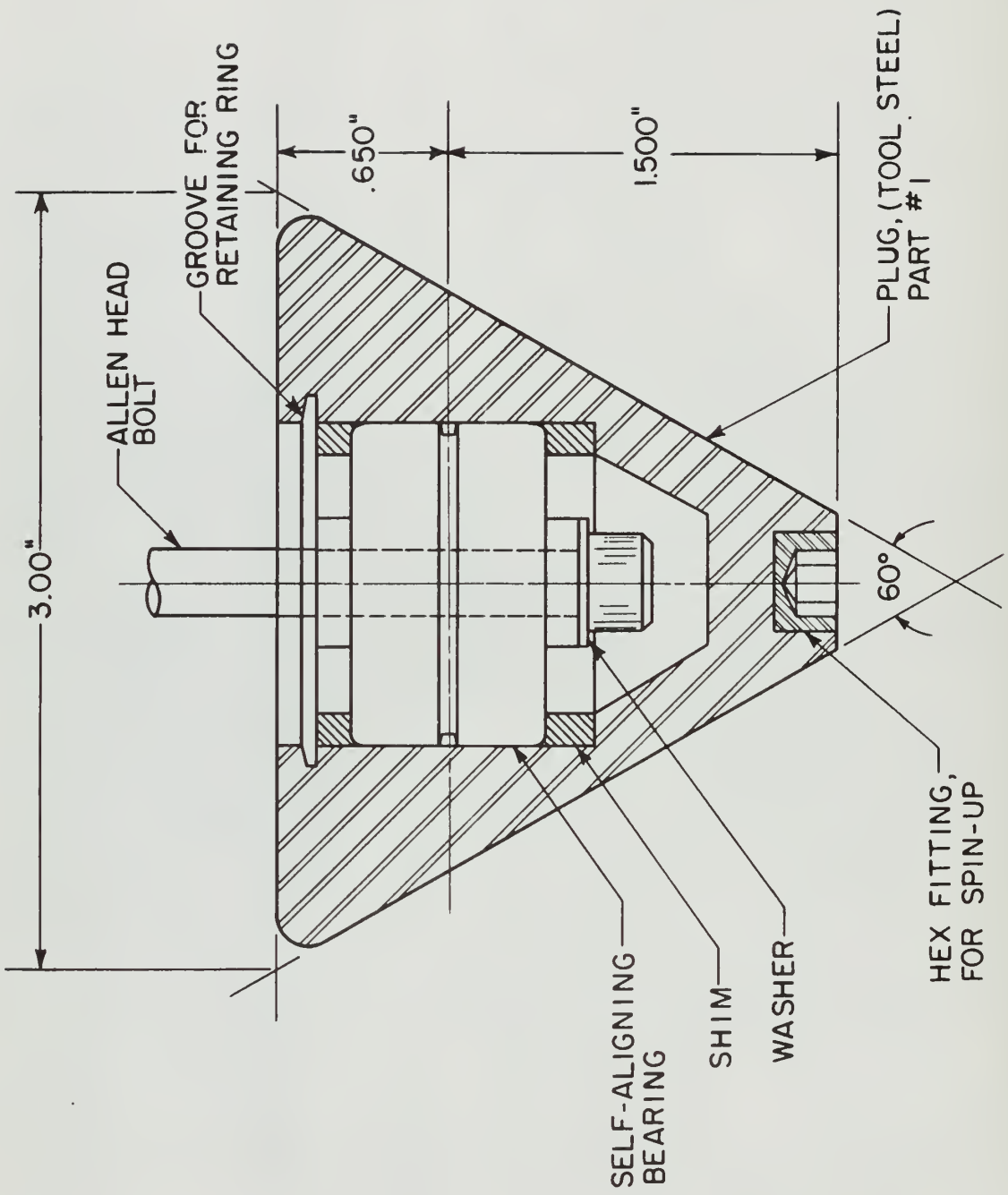

Figure 10. Plug #1, design details

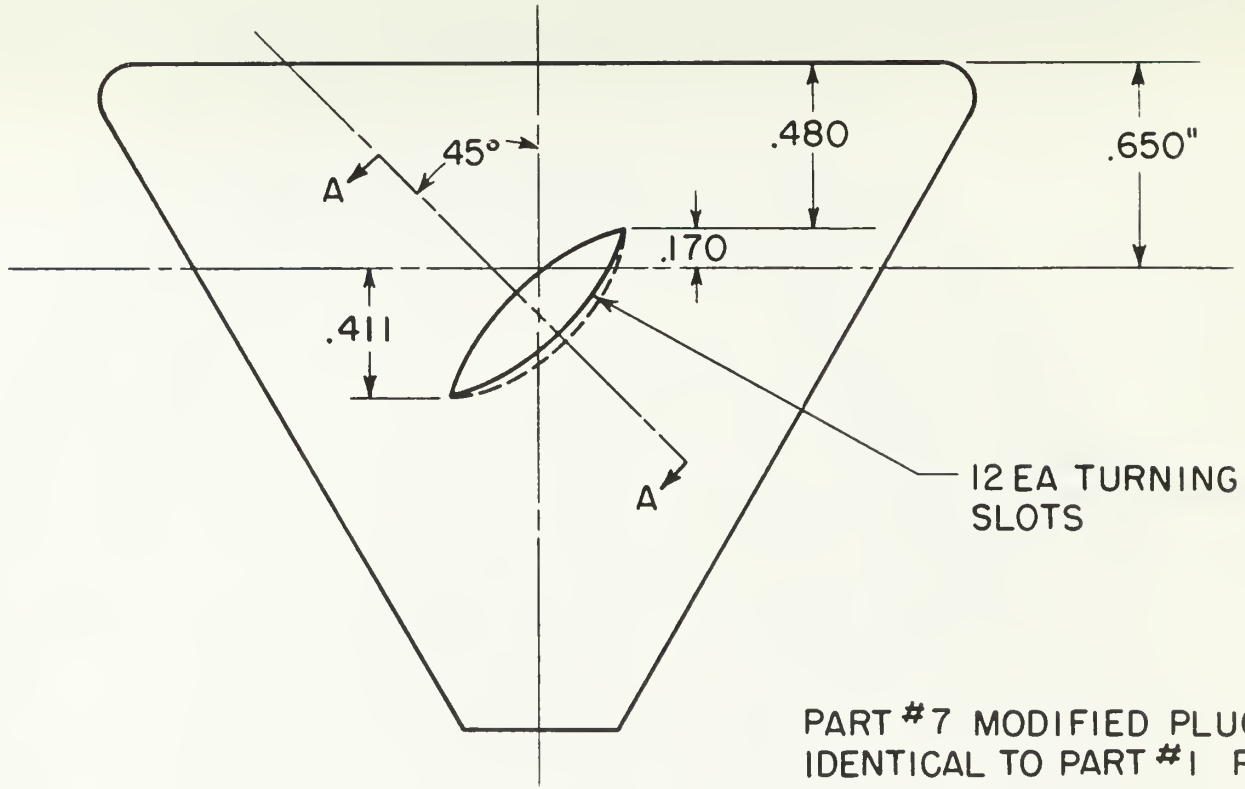

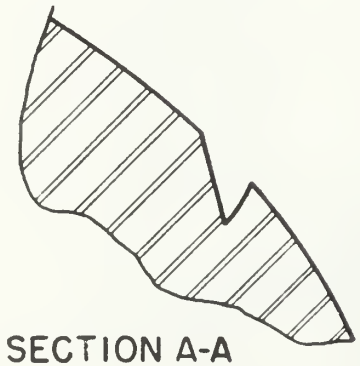

Figure 11. Plug #2, design details

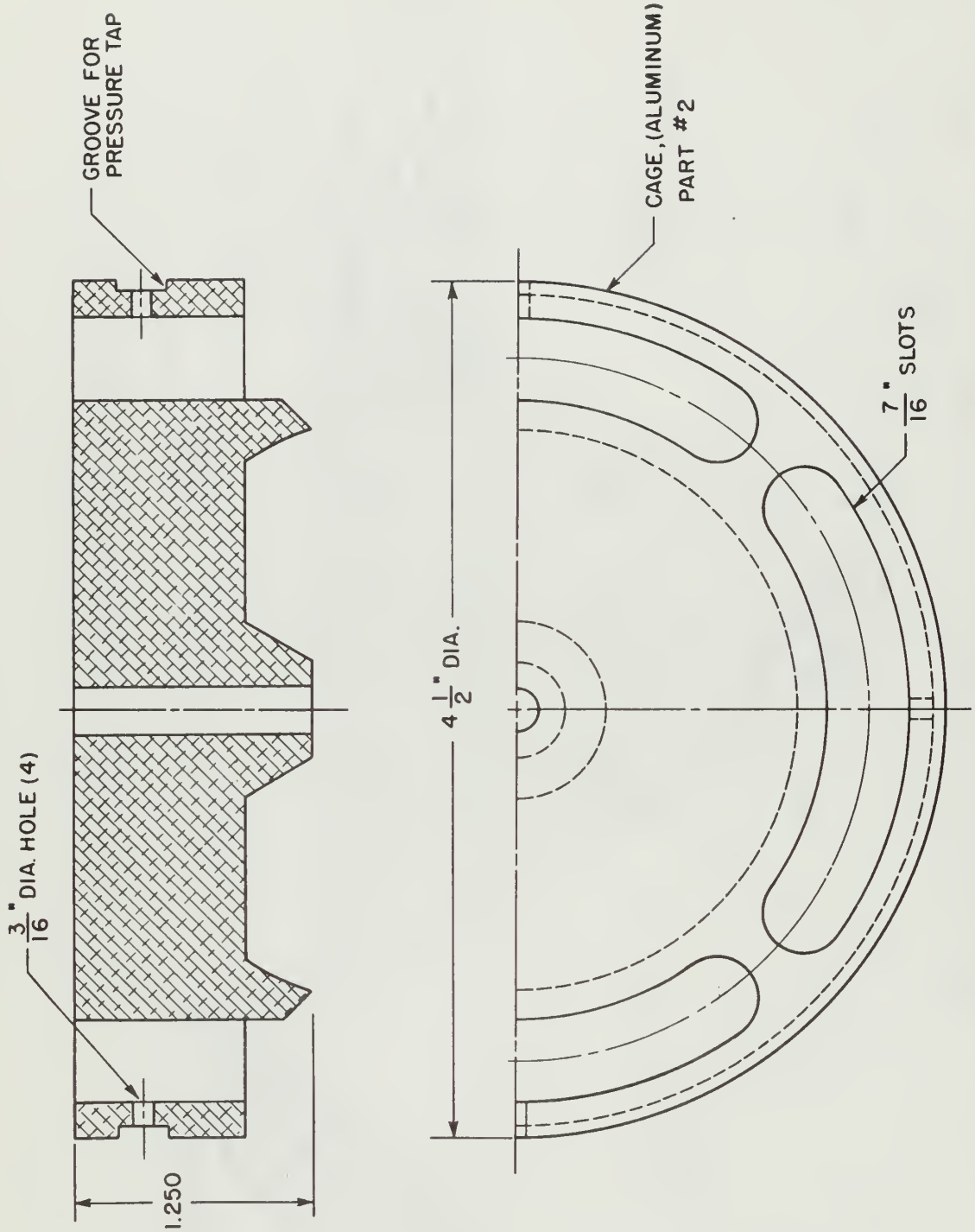

Figure 12. Cage, design details

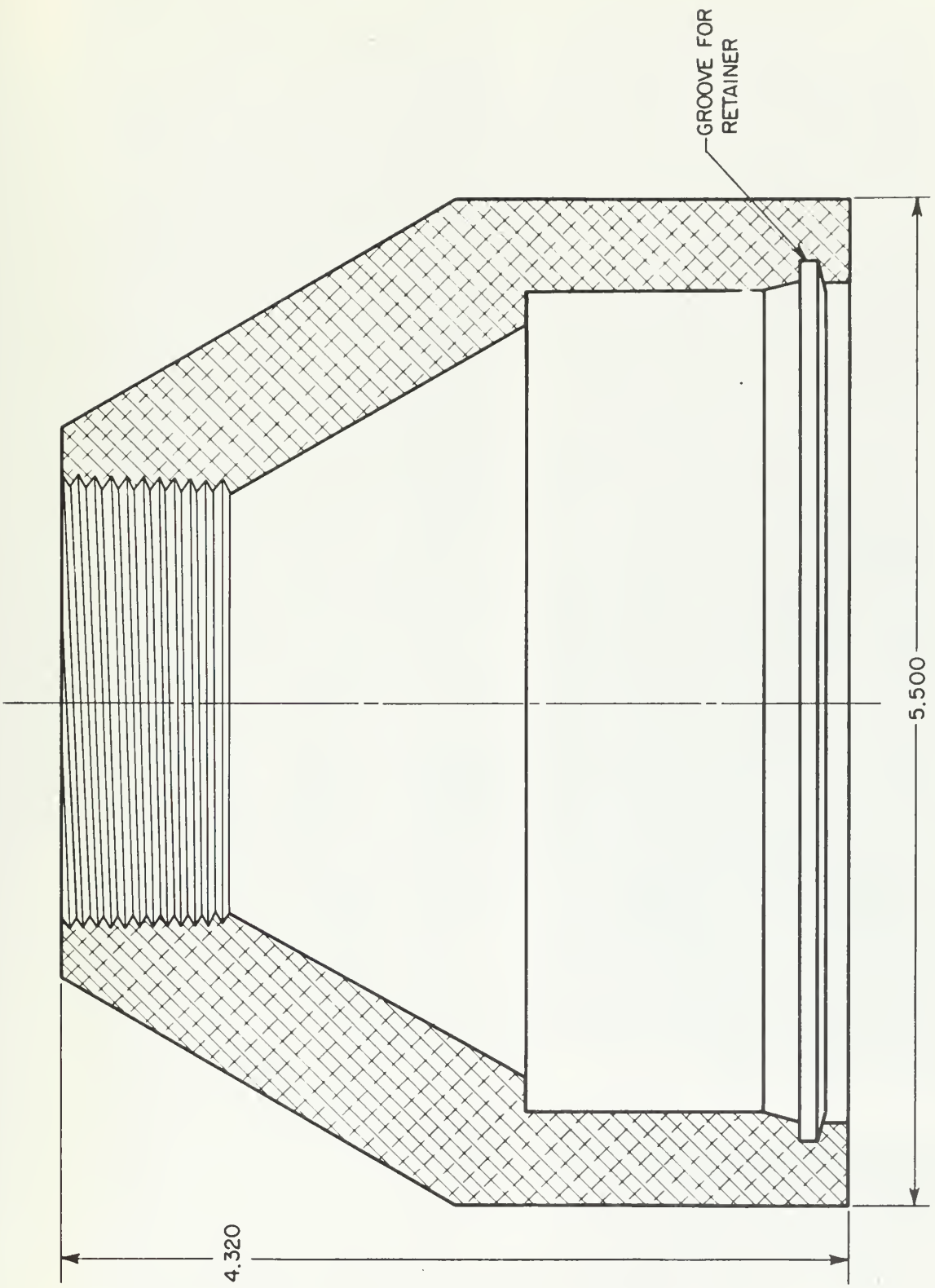

Figure 13. Casing, design details

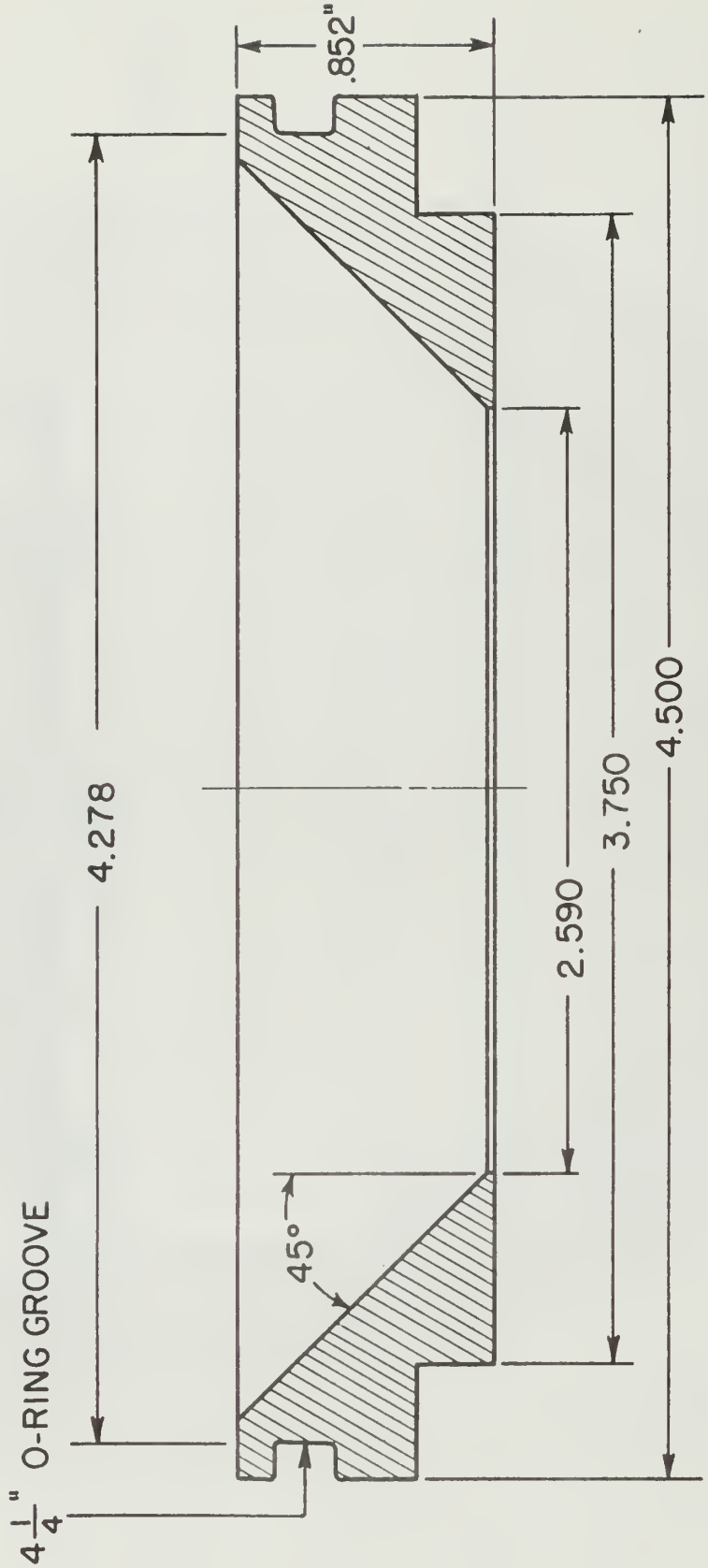

Figure 14. Orifice plate, design details

Figure 15. Plug nozzle test rig

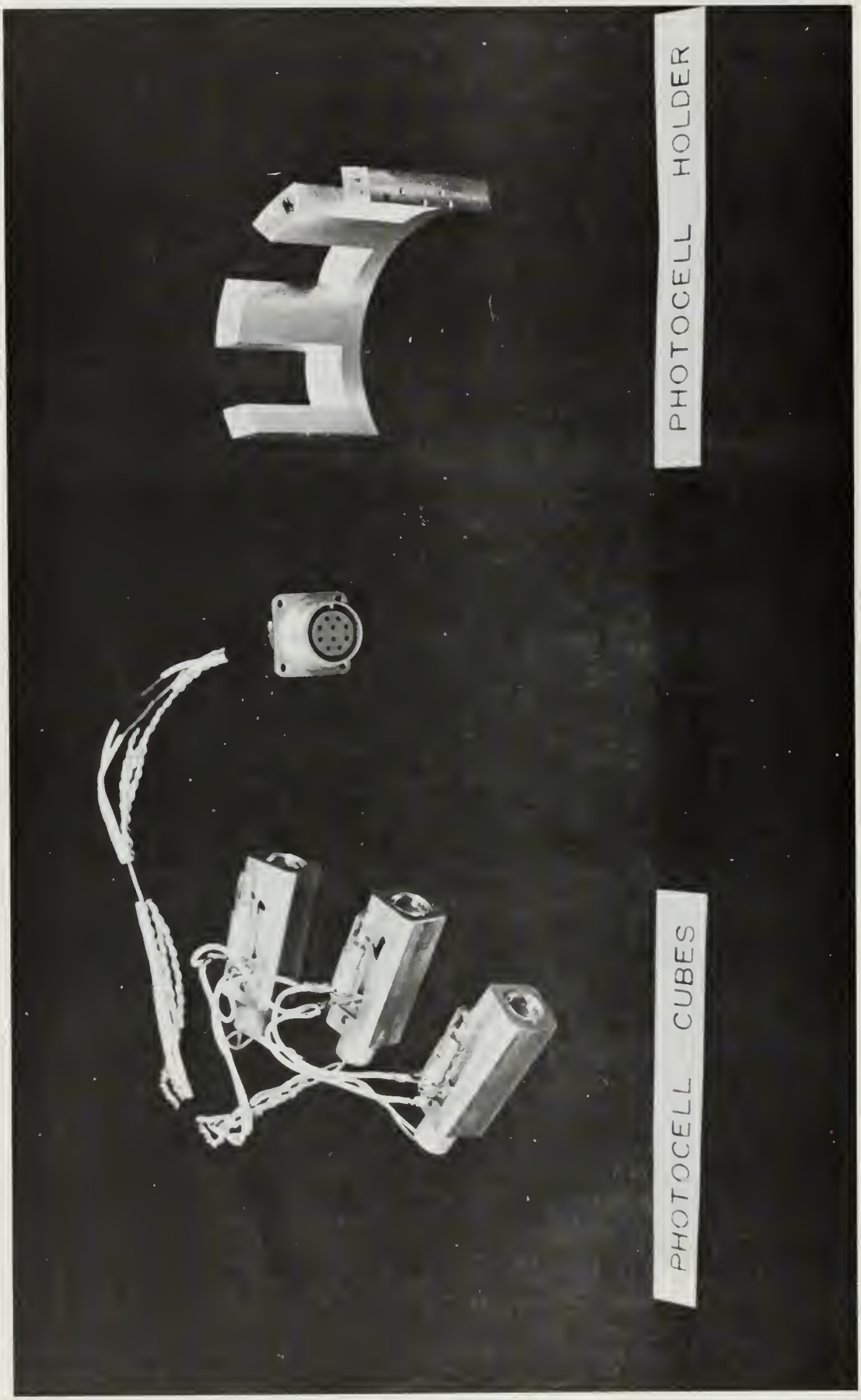

Figure 16. Photocell instrumentation package, disassembled

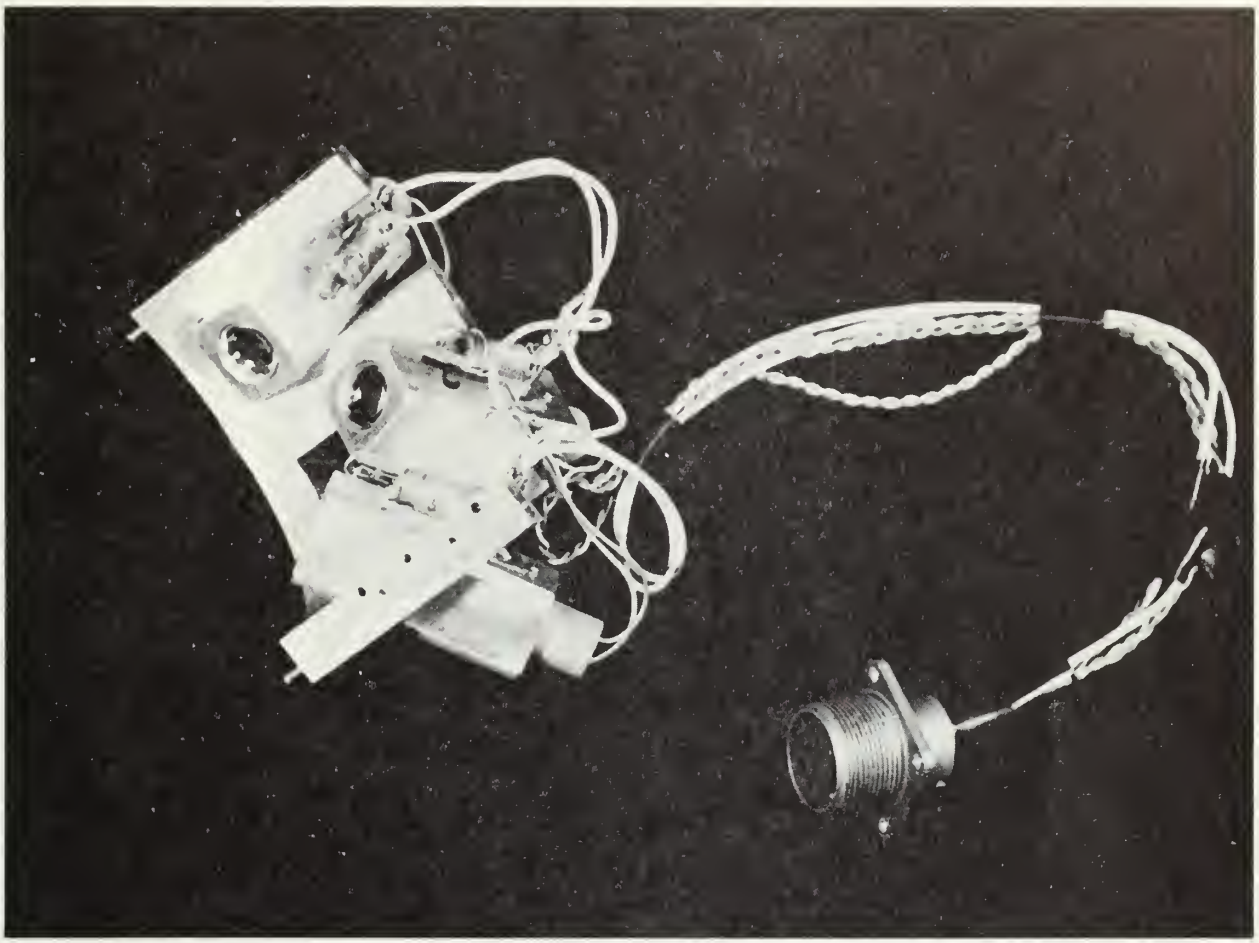

Figure 17. Photocell instrumentation package, assembled

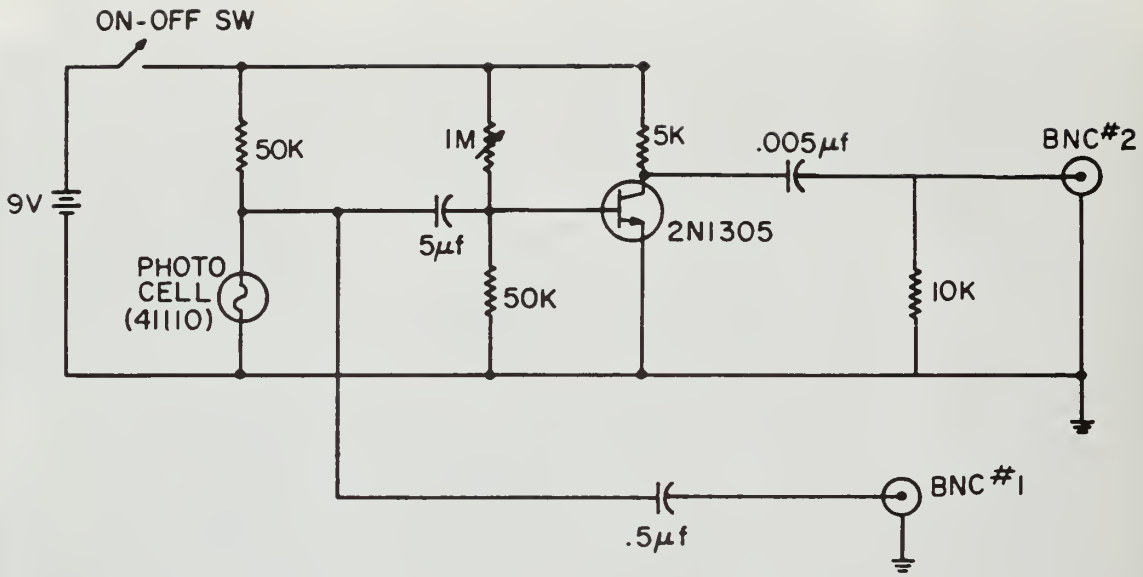

Figure 18. RPM circuit diagram

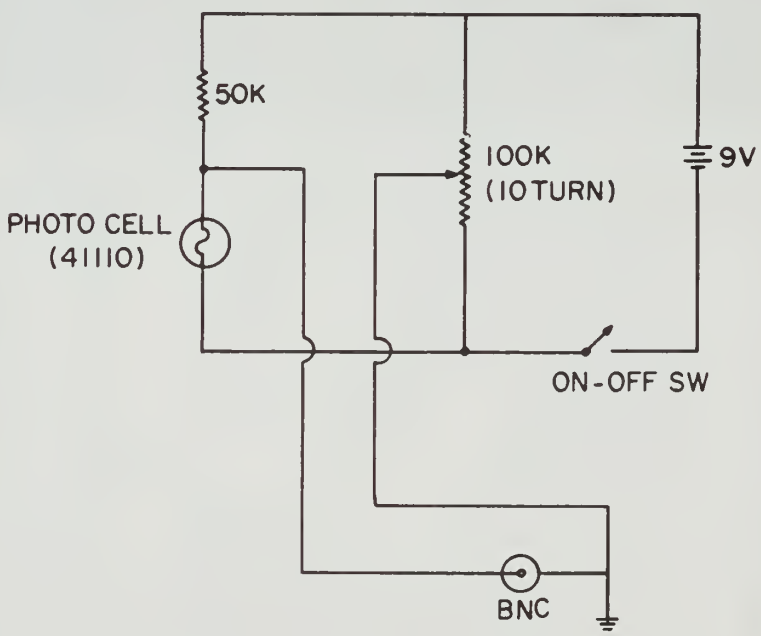

Figure 19. Plug angle circuit diagram

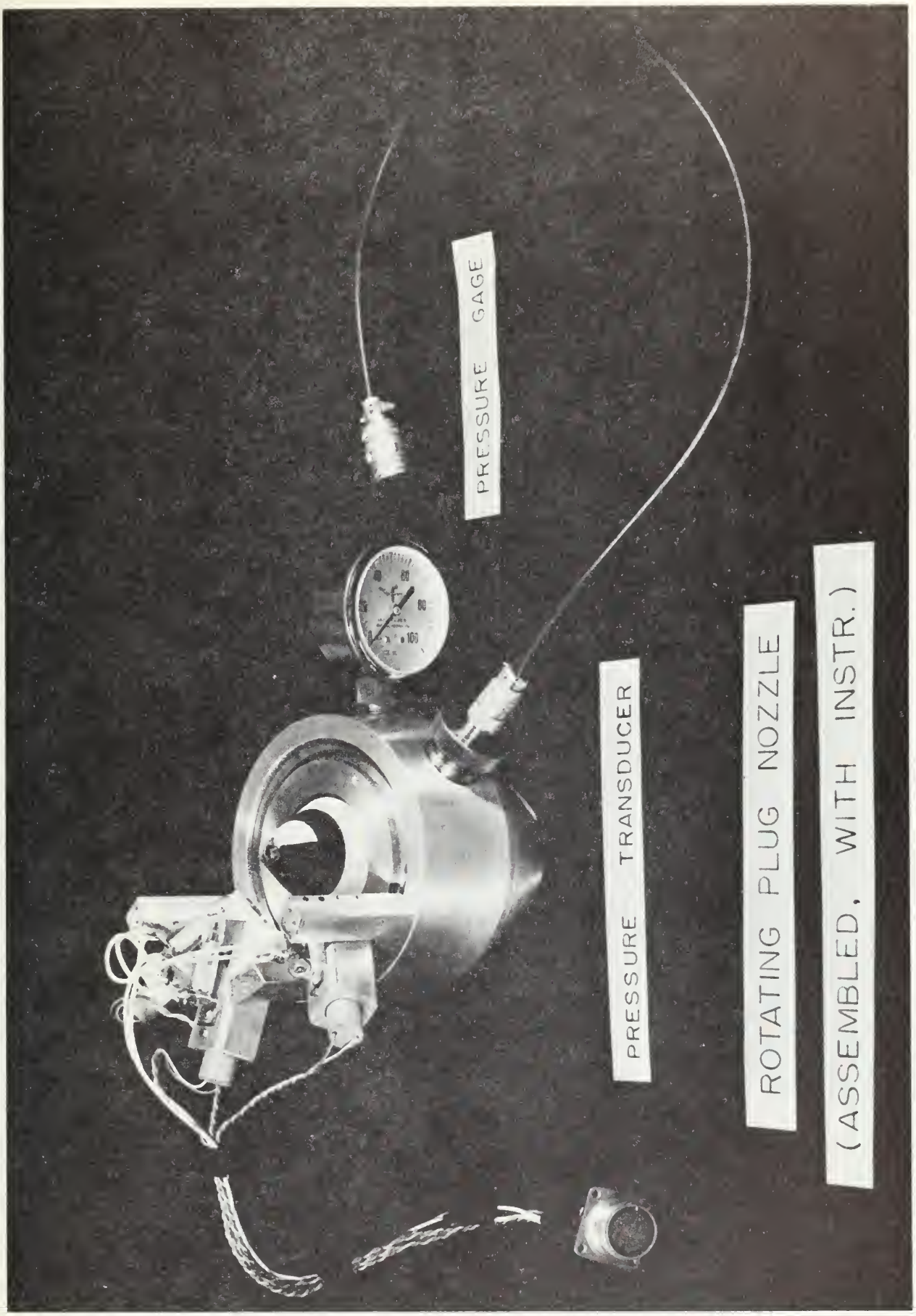

Figure 20. Instrumentation assembled, on casing

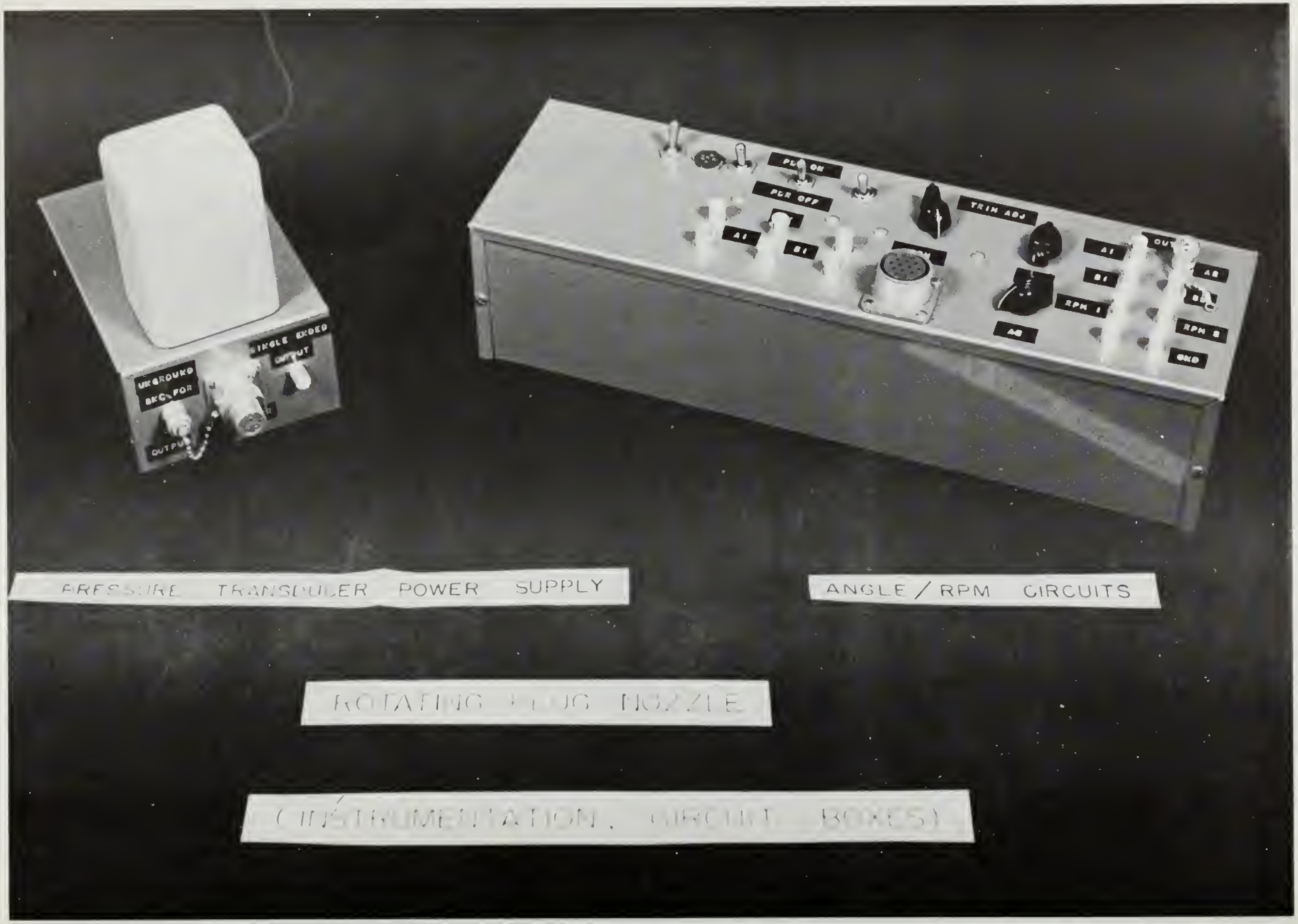

Figure 21. Pressure transducer power supply and angle/RPM circuits

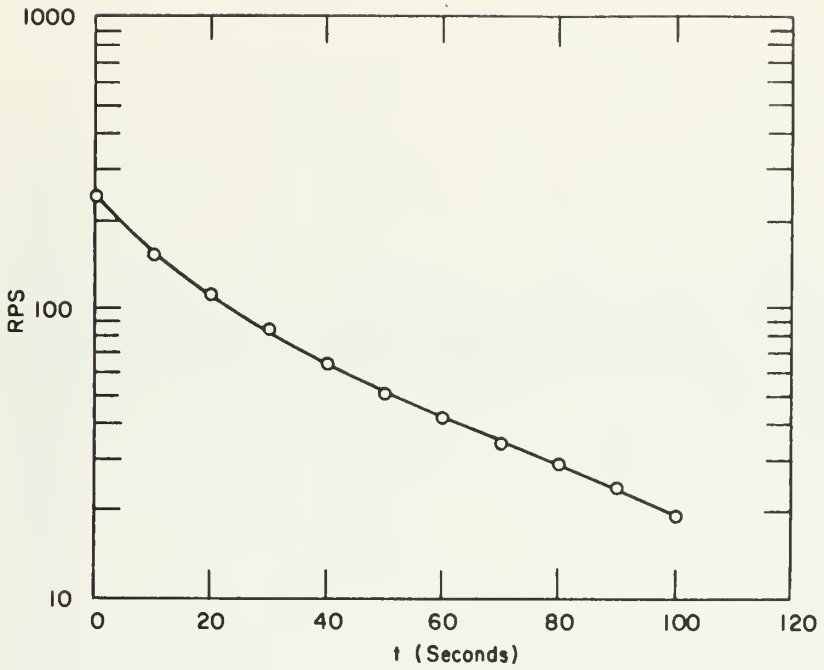

Figure 22. Plug #1 Spin-down test
(Bearing unloaded)
(Light spindle oil)

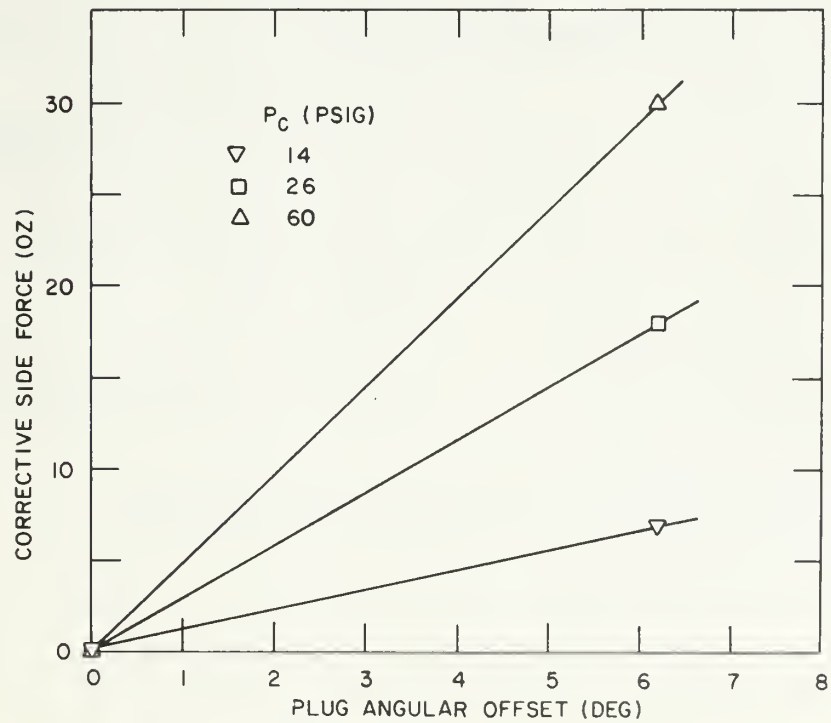

Figure 23. Corrective side force vs. plug angular offset (Plug #1)

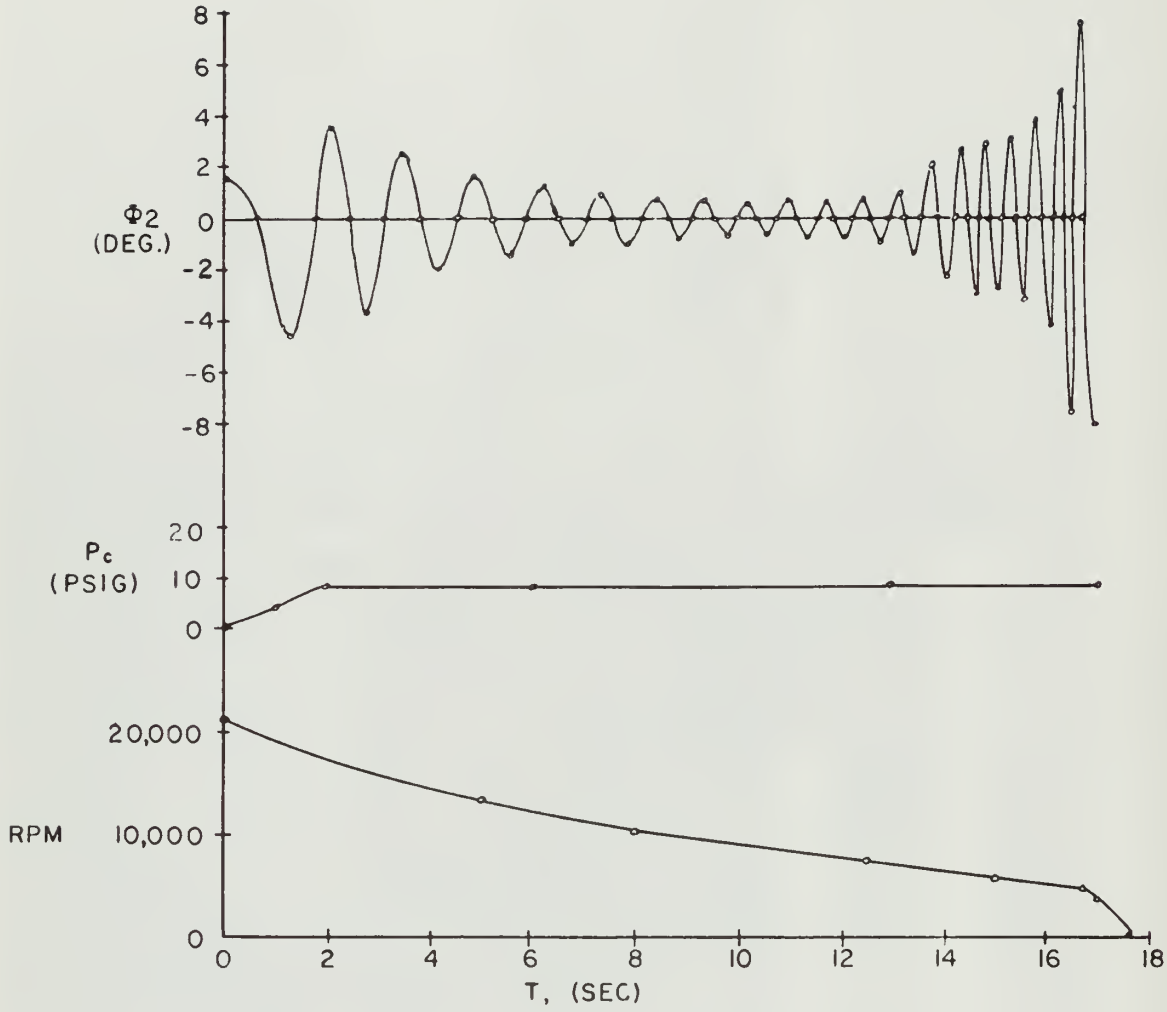

Figure 24. Run no. 4, measured data

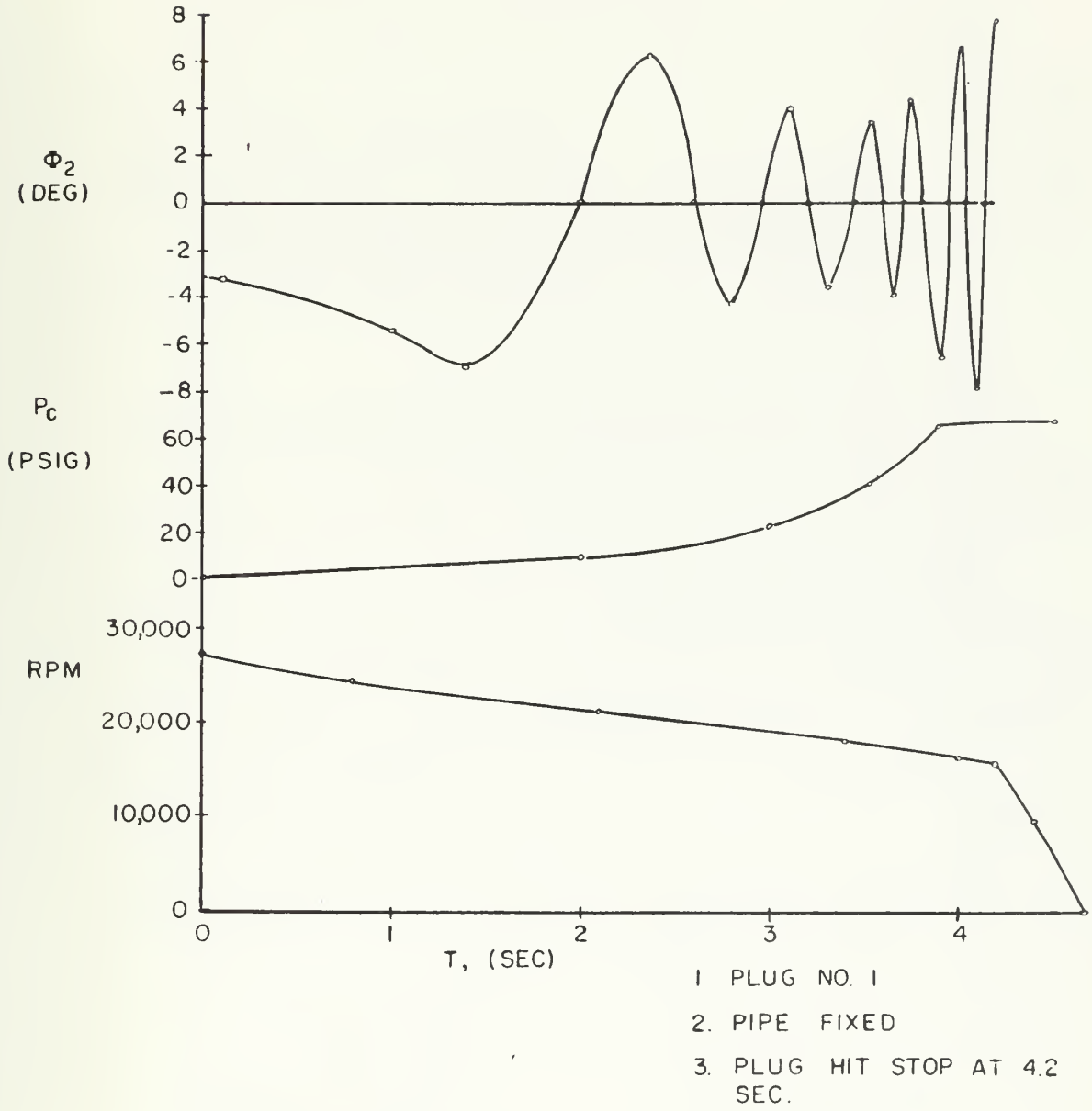

Figure 25. Run no. 5, measured data

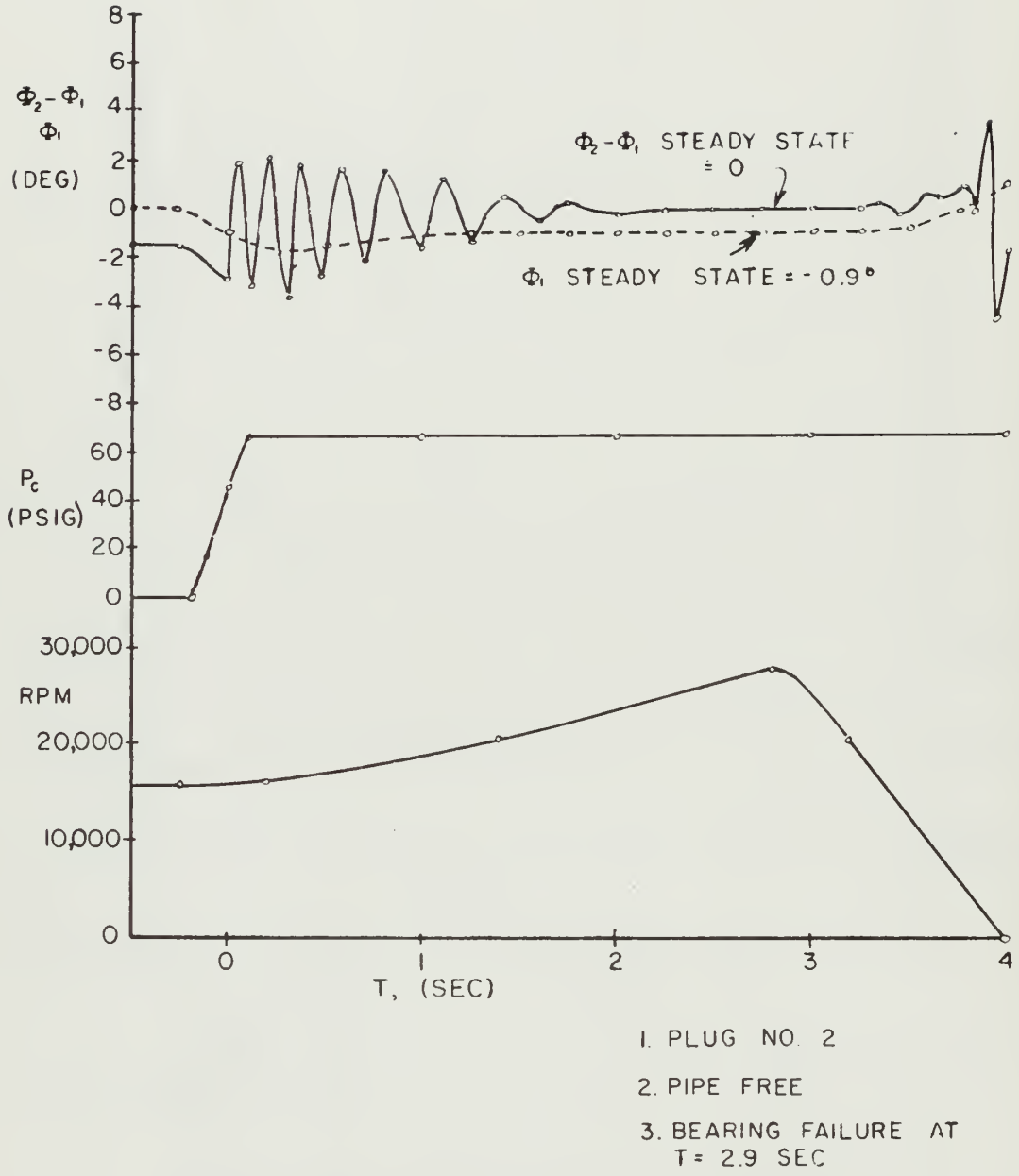

Figure 26. Run no. 12, measured data

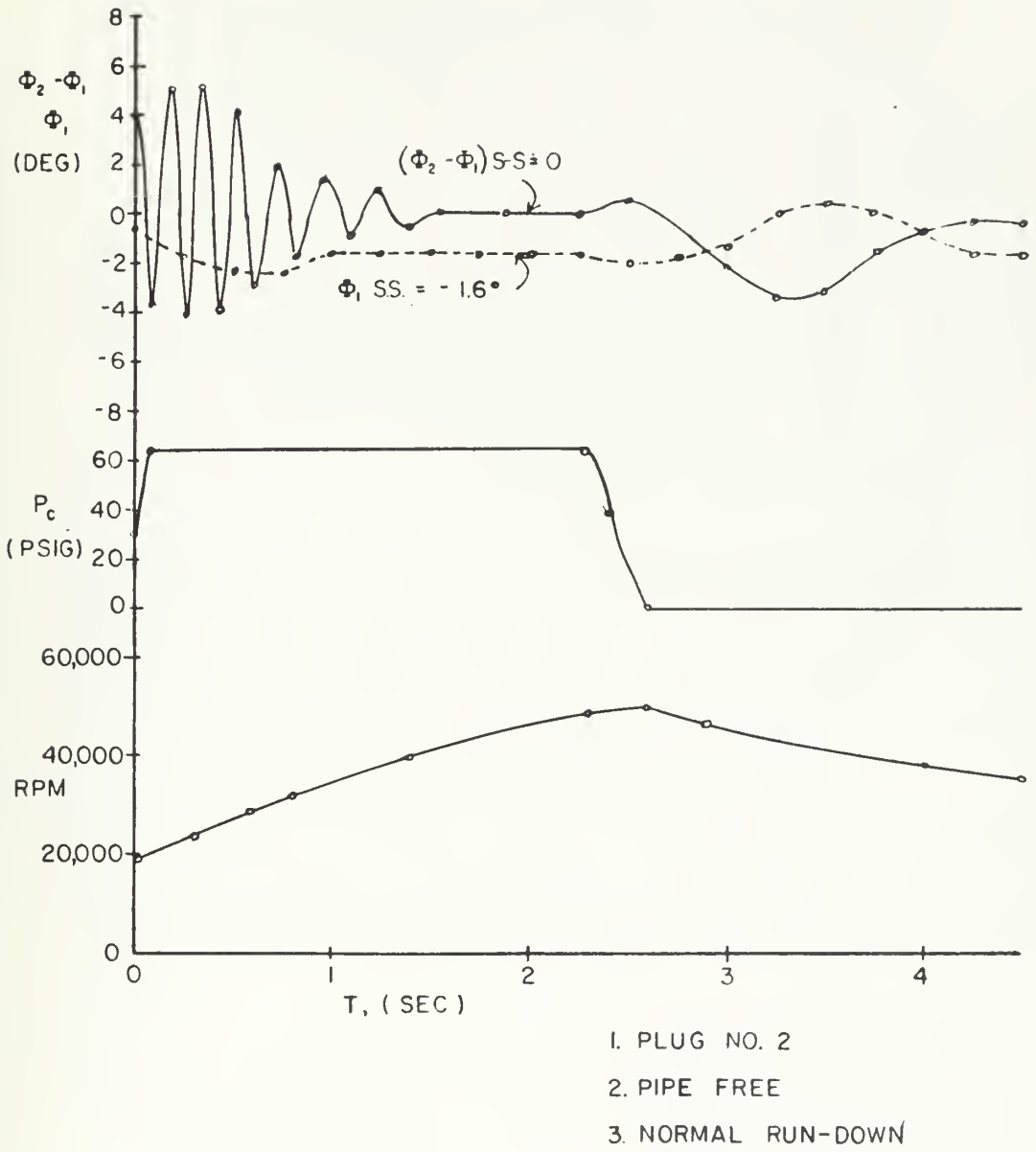

Figure 27. Run no. 14, measured data

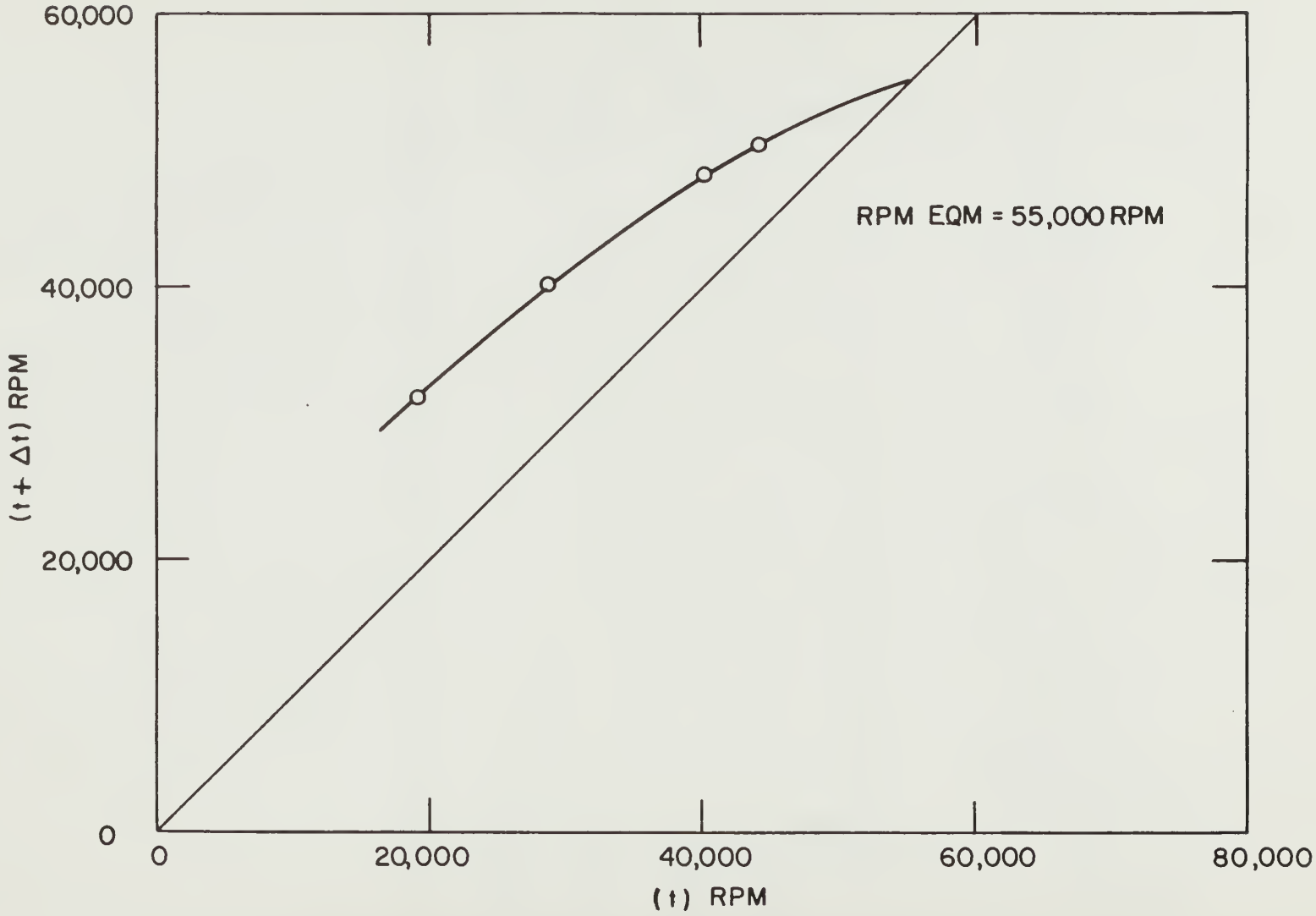

Figure 28. Plug #2 equilibrium RPM (using Mangelsdorf method)

BIBLIOGRAPHY

1. Conrad, G. R., Gleyre, H. R., Ottesen, J., Hu, A. S., "A Control System for Reducing Dispersion of Multi-Stage Sounding Rockets" from Preprints of Papers, Unguided Rocket Ballistics Meteorology Conference, 31 October - 2 November 1967, New Mexico State University, ECOM, U. S. Army Electronics Command.
2. Berman, K., Crimp, F. W. Jr., "Performance of Plug-Type Rocket Exhaust Nozzles," ARS JOURNAL, January 1961.
3. Casci, C., Gismond, E., and Angelino, G., "An Experimental Study on the Application of the Plug Nozzle to Solid Propellant Rockets - 2", SPACEFLIGHT, January 1968.
4. Goldstein, H., Classical Mechanics, Addison-Wesley Publishing Co., Inc., Reading, Mass.
5. Scarborough, J. B., The Gyroscope, Interscience Publishing Co., New York, 1958.
6. Hildebrand, F. B., Method of Applied Mathematics, Prentice-Hall, Inc., New York
7. Thomson, W. T., and Reiter, G. S., "Jet Damping of a Solid Rocket: Theory and Flight Results," AIAA JOURNAL, Vol 3, No. 3, March 1965.
8. Berman, K., Crimp, F. W. Jr., ibid.
9. Krull, H. G. and Beale, W. T., "Comparison of Two Methods of Modulating the Throat Area of Convergent Plug Nozzles," NACA RESEARCH MEMORANDUM, NACA RM E55L08, 1954 (declassified).
10. Krull, H. G. and Beale, W. T., "Effect of Outer-Shell Design on Performance Characteristics of Convergent-Plug Exhaust Nozzles," NACA RM E54K22, 1954 (declassified).
11. Scarborough, J. B., ibid., p 84.
12. Manglesdorf, P. C. Jr., "Convenient Plot for Experimental Functions with Unknown Asymptotes," J. APPL. PHYS., March 1953.

TECHNICAL REPORT DISTRIBUTION LIST

MIT Contract N00014-67-A-0204-0028 - NR 094-362

Rotating Plug Nozzle for Rocket Altitude Control

Recipient	No. of Copies
Defense Documentation Center Cameron Station Alexandria, Virginia 22314	20
Chief of Naval Research Department of the Navy Washington, D. C. 20360 Attn: Mr. J. R. Patton, Jr. Code 473	3
Director Naval Research Laboratory 4555 Overlook Avenue, S. W. Washington, D. C. 20390 Attn: Technical Information Officer	6
U. S. Army Ballistic Missile Agency Huntsville, Alabama 35809	1
U. S. Army Ballistic Research Laboratory Aberdeen Proving Ground, Maryland 21005	1
Director Office of Naval Research Branch Office 495 Summer Street Boston, Massachusetts 02210	1
Director Naval Weapons Laboratory Dahlgren, Virginia 22448 Attn: Technical Library	1
Central Intelligence Agency Washington, D. C. 20505	1
Hercules, Inc. Alleghany Ballistics Laboratory P. O. Box 210 Cumberland, Maryland 21502 Attn: Technical Library	1
Lockheed Propulsion Company P. O. Box 111 Redlands, California 92337	1

Recipient	No. of Copies
North American Rockwell Corporation Rocketdyne Division McGregor, Texas 76657	1
U. S. Army White Sands Missile Range White Sands, New Mexico 88002	1
Director Project SQUID Jet Propulsion Center School of Mechanical Engineering Purdue University Lafayette, Indiana 47907	1
Commander Naval Air Systems Command Department of the Navy Washington, D. C. 20360 Attn: NAVAIR 330 NAVAIR 536, 5366 NAVAIR 604	3
Commander Naval Ordnance Systems Command Department of the Navy Washington, D. C. 20360 Attn: NAVORD 0331	1
Army Missile Command Research and Development Directorate Redstone Arsenal, Alabama 35809 Attn: Propulsion Laboratory	1
Director Applied Physics Laboratory 8621 Georgia Avenue Silver Spring, Maryland 20910 Attn: Library	1
Commander Air Force Systems Command Andrews Air Force Base Silver Hill, Maryland 20331	1

Recipient	No. of Copies
Commander Air Force Rocket Propulsion Laboratory Edwards Air Force Base, California 93523	1
Commander Air Force Aero Propulsion Laboratory Wright-Patterson Air Force Base Dayton, Ohio 45433	1
National Aeronautics and Space Administration Lewis Research Center 21000 Brookpark Road Cleveland, Ohio 44135 Attn: Library	1
Naval Missile Center Point Mugu, California 93041 Attn: Technical Library Code 5632.2	1
U. S. Naval Postgraduate School Monterey, California 93940 Attn: Library, Code 0212 Section 2124	1
Headquarters Naval Material Command Special Projects Office Washington, D. C. 20360 Attn: Technical Library	1
United Aircraft Corporation 400 Main Street East Hartford, Connecticut 06118 Attn: Engineering Department	1
United Aircraft Corporation Pratt and Whitney Aircraft Division P. O. Box 2691 West Palm Beach, Florida 33402 Attn: Head Librarian	1
Commander Air Force Office of Scientific Research 1400 Wilson Boulevard Arlington, Virginia 22209 Attn: Dr. J. F. Masi	1

Recipient	No. of Copies
Atlantic Research Corporation Shirley Highway at Edsall Road Alexandria, Virginia 22314 Attn: Dr. R. Friedman Director of Research	1
Chemical Propulsion Information Agency The Johns Hopkins University Applied Physics Laboratory Silver Spring, Maryland 20910	1
Thiokol Chemical Corporation Reaction Motors Division Denville, New Jersey 07834 Attn: Director of Research	1
Aerojet-General Corporation P. O. Box 15847 Sacramento, California 95813 Attn: Director of Research	1
Director of Defense Research and Engineering Technical Library Room 3C128, The Pentagon Washington, D. C. 20301 Attn: Propulsion Technology	1
Chief of Research and Development Headquarters, Department of the Army Washington, D. C. 20310 Attn: Dr. S. J. Magram Physical and Engineering Division	1
Naval Weapons Center China Lake, California 93555 Attn: Technical Library	1
California Institute of Technology Jet Propulsion Laboratory 4800 Oak Grove Drive Pasadena, California 91103	1
Naval Ordnance Laboratory White Oak Silver Spring, Maryland 20910 Attn: Research Director	1

Recipient	No. of Copies
Rocketdyne A Division of North American Rockwell Corporation Department 895, Zone 7 6633 Canoga Avenue Canoga Park, California 91304	1
Naval Air Systems Command Room 3814, Munitions Building Washington, D. C. 20360 Attn: Dr. H. Rosenwasser, AIR 310C	1
Navy Underwater Sound Laboratory Fort Trumbull New London, Connecticut 06320 Attn: Technical Library	1
Bureau of Naval Personnel Department of the Navy Washington, D. C. 20370 Attn: Technical Library	1
U. S. Naval Oceanographic Office Suitland, Maryland 20390 Attn: Library, Code 1640	1
Naval Ship Engineering Center Philadelphia Division Philadelphia, Pennsylvania 19112 Attn: Technical Library	1
Naval Applied Science Laboratory Flushing and Washington Avenues Brooklyn, New York 11251 Attn: Technical Library, Code 222	1
Naval Ship Research and Development Center Annapolis Division Annapolis, Maryland 21402 Attn: Library, Code A214	1
Naval Undersea Warfare Center 3202 East Foothill Boulevard Pasadena, California 91107 Attn: Technical Library	1
Naval Ship Systems Command Room 1532, Main Navy Washington, D. C. 20360 Attn: Technical Library	1

Unclassified

Security Classification

DOCUMENT CONTROL DATA - R & D

(Security classification of title, body of abstract and indexing annotation must be entered when the overall report is classified)

1. ORIGINATING ACTIVITY *(Corporate author)*

Aerophysics Laboratory
Massachusetts Institute of Technology
560 Memorial Drive, Cambridge, Mass 02139

2a. REPORT SECURITY CLASSIFICATION

Unclassified

2b. GROUP

3. REPORT TITLE

ATTITUDE STABILIZATION USING A ROTATING PLUG NOZZLE

4. DESCRIPTIVE NOTES *(Type of report and inclusive dates)*

Final (MIT EAA Thesis) 1 January to 30 June 1969

5. AUTHOR(S) *(First name, middle initial, last name)*

JOHN E. DRAIM, CAPT., USN

6. REPORT DATE

JULY 1969

7a. TOTAL NO. OF PAGES

88

7b. NO. OF REFS

12

8a. CONTRACT OR GRANT NO.

N00014-67-A-0204-9928

b. PROJECT NO.

c. NR 094-362/10-9-68(473)

d.

9a. ORIGINATOR'S REPORT NUMBER(S)

TR 158

9b. OTHER REPORT NO(S) *(Any other numbers that may be assigned this report)*

10. DISTRIBUTION STATEMENT

Qualified requestors may obtain copies of this report from the Defense Documentation Center.

11. SUPPLEMENTARY NOTES

12. SPONSORING MILITARY ACTIVITY

Office of Naval Research
Department of the Navy
Washington, D.C. 20360

13. ABSTRACT

A modified plug nozzle in which the plug is spinning as a gyroscopic mass is investigated. Exhaust gas flow is modulated between the plug and the rocket casing in such a manner as to provide a stabilizing moment around the rocket center of gravity. Lagrange equations of motion are formulated for the dynamical system. These equations are mechanized in an analog computer to yield plots of rocket angular motions. Critical non-dimensional parameters for the system are identified and discussed. A small demonstrator model was designed, constructed and tested; conical plug had indented turning slots in the area of the exhaust annulus. Tests conducted on the model demonstrated that sufficient gyroscopic rigidity can be generated to counter the unbalanced pressure field effects around the rotating plug. It is concluded that within certain limits of the critical parameters, satisfactory attitude stabilization of a rocket vehicle can be realized using a rotating plug-type nozzle.

DD FORM 1 NOV 65 1473

Unclassified

Security Classification

14 KEY WORDS	LINK A		LINK B		LINK C	
	ROLE	WT	ROLE	WT	ROLE	WT
STABILITY, ROCKET						
CONTROL, ATTITUDE						
PLUG NOZZLE						
NOZZLE						
GUIDANCE, STRAIGHT LINE						
STABILIZATION, ROCKET VEHICLES						
THRUST VECTORING, ROCKET						
SPIN STABILIZATION						
STABILIZATION, ATTITUDE						
ROCKET						
PROBE ROCKET						
ATTITUDE CONTROL						


MASSACHUSETTS
INSTITUTE OF TECHNOLOGY
1861
MENS ET MANUS